Chapter 6

TWO-DIMENSIONAL MHD CODE

Tatsuki Ogino

6.1 Introduction

6.1.1 General remarks on tutorial course on MHD simulation

It is not easy to understand the solar-terrestrial phenomena from only the limited measurements provided by spacecraft or from only the pure theories. This is because the solar-terrestrial phenomena have three particular features which are characterized by the high nonlinearity, the strong inhomogeneity and the great temporal variations from a steady state. For example, large amplitude disturbances frequently propagate in the interplanetary space, and a large amount of energy is stored in the earth's magnetotail, then it is suddenly released. During the past decade a new technique, a computer simulation which uses a fluid model including a magnetohydrodynamic (MHD) model, has been developed to solve for the solar-terrestrial phenomena and to provide a self-consistent picture of the solar-terrestrial system and physical processes in it. The three-dimensional global MHD simulation of the interaction between the solar wind and the earth's magnetosphere is a typical example to solve the solar-terrestrial system, and the local MHD simulations for the magnetic reconnection and Kelvin-Helmholtz instability are two typical examples to make clear the physical processes in space physics.

The fluid and MHD simulation codes have been well developed to handle the particular subject in space physics by introducing new numerical methods, and the diagnostic tools have also progressed in graphic software to help the understandings of simulation results. Thus we have been able to reach a new stage that the simulation results by a supercomputer have some meaning in comparison with the realistic phenomena. However, those simulation codes must be developed furthermore in order to treat a more realistic problem in

the solar-terrestrial phenomena, to quantitatively compare with observational results, and also to bring a fruitful understanding in space physics.

In the present stage, we want to arrange the basic ideas of numerics and to present several fundamental numerical methods which were used as starting points in the fluid and MHD simulations in space physics. Then, I will mention about several recent developments in numerical methods and MHD codes, and also successful applications to simple space physics problems. These include several numerical algorithms such as implicit-explicit schemes, leap-frog scheme, two-step Lax-Wendroff scheme and other improved schemes to solve the linear and nonlinear wave propagations in one dimension. By a two-dimensional MHD code based on the two-step Lax-Wendroff method, the magnetic reconnection is simulated as an example of local processes and the solar wind and earth's magnetosphere interaction is simulated as an example of global simulations. This fundamental course of the fluid and MHD codes will be useful for beginners to understand the simple idea and technique of simulations and also for scientists of ripe experience to grasp an essential and unified idea of numerics and a future direction of global MHD simulation.

6.1.2   A survey of global MHD simulations

As was mentioned previously, it is not easy to investigate an interaction process between the solar wind and the earth's magnetosphere or a magnetospheric system because the observations are temporarily and spatially limited to the spacecraft trajectory. In order to understand a magnetospheric system, the experimenter is challenged to interpret the limited single point measurements in terms of a large-scale and highly dynamic system. During the past several years a new technique, computer simulation by using the global magnetohydrodynamic (MHD) model, has been developed to solve the magnetospheric configuration and to present a self-consistent picture of the solar wind-magnetosphere interaction process.

The first work on the time-dependent global MHD simulation of the earth's magnetosphere was done by Leboeuf et al. [1978] to produce a interplanetary magnetic field (IMF), where a 2 dimensional MHD particle code was used. Leboeuf et al. [1981] successively developed their 2 dimensional MHD particle code to a 3 dimensional code and again reproduced a similar topology. The MHD particle code has an advantage to be numerically stable without adjustment of the time step there. However, the plasma sheet was short (about $-30R_e$) due to the effect of a large numerical magnetic diffusion, where R_e is the radius of earth and the earth's magnetosphere was simulated by using a minimally diffusive MHD code to show the basic features of the magnetosphere such as the bow shock, magnetopause and long magnetotail [Lyon et al., 1980]. They used the flux-corrected transport (FCT) for the hydrodynamic variables and the partial donor cell method (PDM) for the magnetic field. Lyon et al. [1981; 1986]

modified the MHD code and applied to simulate a substorm-like process occurring in the earth's magnetosphere, where a leapfrog time-integration scheme, a 20th-order finite difference approximation to the spatial derivatives and flux-corrected transport were used. As the result, the MHD code could produce a long magnetotail (more than $-60R_e$) and obtained the simulation results consistent with an empirical substorm model namely the near-earth magnetic neutral-line model depending on the resistive terms.

Brecht et al. [1981; 1982] developed the MHD code to a 3 dimensional version to study the 3 dimensional feature of the interaction between the solar wind and the earth's magnetosphere where the partial donor cell method was used on the inhomogeneous grids. As the result they could successfully treat a longer magnetotail ($-90R_e$) as well as the sharp gradients of the bow shock, the stagnation point and the magnetopause in the dayside interaction region. Wu et al. [1981] simulated the steady state magnetospheric configuration to reproduce many of the magnetospheric features such as the bow shock, magnetopause and plasma sheet at a quiet time by using a 3 dimensional MHD model, where the Rusanov scheme was used. He applied the MHD model to study the shape of the magnetosphere [1983] and the effect of dipole tilt on the magnetospheric structure [1984].

The interaction of the solar wind with the earth's magnetosphere was also studied by using a different time-dependent 3 dimensional MHD model by Ogino and co-workers [Ogino, 1986; Ogino and Walker, 1984; Ogino et al., 1985; 1986] where a modified two step Lax-Wendroff scheme was adopted. They tried to project the physical quantities such as the parallel vorticity and field aligned currents onto the polar cap along magnetic field lines in order to compare with the observations and demonstrated the projected patterns of the magnetospheric convection system and field aligned currents depending on the IMF orientation. The nature of the solar wind-magnetosphere- ionosphere coupling was also simulated by Fedder and Lyon [1987] in order to investigate the physics and behavior of the controlling processes. They showed the current-voltage relationship in the magnetosphere as a dynamo process and discussed the operation of the dynamo and its location. Watanabe and Sato [1990] developed a new 3 dimensional MHD code based on the fourth-order Runge-Kutta-Gill time advance and the direct finite space difference and applied to the study of the solar wind interaction with the earth's dipole field. The method has an advance to keep a long time step of difference.

The tearing mode at the dayside magnetopause was successively investigated by 2-dimensional computer simulations of stagnation-region flow toward a current sheet [Fu and Lee, 1985], coupling with Kelvin-Helmholtz instability [La Belle-Harmer et al., 1988] and a multiple X line reconnection in a global configuration [Shi et al., 1988]. However, their MHD simulations were limited to an incompressible and 2-dimensional case. Scholer [1988] and Southwood et al. [1988] have suggested that the reconnection associated with FET's occurs at

a single location but is time dependent. Sato et al. [1986] demonstrated a magnetic flux tube created as a result of repeated reconnection between the IMF and geomagnetic field by using a semi-global MHD model. Ogino et al. [1989a, 1990] modeled the generation of magnetic flux ropes at the magnetopause and in the magnetotail from a global MHD simulation.

Global MHD simulation codes have been used to model magnetosphere other than the Earth's magnetosphere. Schmidt and Wegmann [1980, 1982; Wegmann *et al.*, 1987], Fedder *et al.* [1984], Ogino *et al.* [1986*a*, 1988*a*] and Sydora and Raeder [1988] investigated cometary magnetospheres. Walker and Ogino [1986] simulated the Jovian magnetosphere. Most recently Linker et al. [1988] developed a model of the interaction of Jovian plasma with the moon Io.

The main purpose of the present lecture note is to study a 2 dimensional MHD code of the global simulation and apply the code to simulation of the interaction between the solar wind and the earth's magnetosphere. We will obtain a quasi-steady state magnetospheric configuration when we change the IMF z-component. The present 2 dimensional MHD code in which the two-step Lax-Wendroff method is used can be of course applied to simulate other physical phenomena in space physics such as nonlinear MHD waves, MHD instabilities, magnetic reconnection and tearing mode. Moreover, an extension to the 3 dimensional MHD code is also briefly mentioned with several examples of the global simulation.

6.2   Global MHD Model of Magnetosphere

A global MHD simulation model of the interaction between the solar wind and the earth's magnetosphere is described in detail in this section [for example refer to papers of Ogino, 1986; Ogino et al., 1985]. The present purpose is to study the MHD simulation code generally. Therefore, we will start with 3-dimensional MHD model because the 2-dimensional model can be straightforward reduced from the 3-dimensional one.

6.2.1   Basic equations

The MHD and Maxwell's equations are solved as an initial value problem by using the two-step Lax-Wendroff scheme [Ogino *et al.*, 1981a]. The normalized MHD equations used in the present simulation are written as follows:

$$\frac{\partial \rho}{\partial t} = -\nabla \cdot (\mathbf{v}\rho) + D\nabla^2 \rho \tag{6.1}$$

$$\frac{\partial \mathbf{v}}{\partial t} = -(\mathbf{v} \cdot \nabla)\mathbf{v} - \frac{1}{\rho}\nabla p + \frac{1}{\rho}\mathbf{J} \times \mathbf{B} + \mathbf{g} + \frac{1}{\rho}\mathbf{\Phi} \tag{6.2}$$

$$\frac{\partial p}{\partial t} = -(\mathbf{v} \cdot \nabla)p - \gamma p\nabla \cdot \mathbf{v} + D_p\nabla^2 p \tag{6.3}$$

$$\frac{\partial \mathbf{B}}{\partial t} = \nabla \times (\mathbf{v} \times \mathbf{B}) + \eta \nabla^2 \mathbf{B} \qquad (6.4)$$

$$\mathbf{J} = \nabla \times (\mathbf{B} - \mathbf{B}_d) \qquad (6.5)$$

where ρ is the plasma density, $\mathbf{v}$ is the flow velocity, p is the plasma pressure, $\mathbf{B}$ is the magnetic field, $\mathbf{J}$ is the current density, $\mathbf{g}$ is the gravity force, $\mathbf{\Phi} \equiv \mu \nabla^2 \mathbf{v}$ is the viscosity, $\gamma = 5/3$ is the ratio of specific heats, $\eta = \eta_0 (T/T_0)^{-3/2}$ is the resistivity with a classical temperature dependence, $T = p/\rho$ is the temperature, T_0 is the ionospheric temperature, and $\mathbf{B}_d$ is the 3-dimensional dipole magnetic field. Typical numerical values are $\eta_0 = 0.01$ and $\mu/\rho_{sw} = 0.02$, where the diffusion coefficients $D = D_p = \mu/\rho_{sw}$. Hence the typical magnetic Reynolds number is $S = \tau_\eta/\tau_A = 50-1000$. Here, the subscript sw indicates the quantities in the solar wind.

The normalization quantities in the basic equations are the radius of the earth, $x_s = R_E = 6.37 \times 10^6$ m, the magnetic field of the earth at one earth radius at the equator, $B_s = 3.12 \times 10^{-5}$ T, the density of the ionosphere, $\rho_s = m n_s (n_s = 10^{10} m^{-3})$, the Alfvén velocity at one earth radius, $v_s = B_s/(\mu_0 \rho_s)^{1/2} = 6.80 \times 10^6$ m/s, and the Alfvén transit time, $t_s = R_E/v_s = 0.937$ s. In such a case, the other normalization quantities are automatically determined as $p_s = \rho_s v_s^2 = B_s^2/\mu_0 = 7.75 \times 10^{-4}$ N/m^2, $J_s = B_s/\mu_0 x_s = 3.90 \times 10^{-6}$ A/m^2, and $g_s = v_s/t_s = 7.26 \times 10^6$ m/s^2. The subtraction of the dipole field in (1e) is performed to suppress the numerical error arising from the difference approximation at the discontinuity. The viscosity and diffusion terms in (1a), (1b), and (1c) were added to reduce the MHD fluctuations which come from an unbalanced force at the initial state. That is, the numerical oscillations on the scale of the mesh size decrease in front of the bow shock when we include the viscosity and diffusion terms. The global magnetospheric configuration is little changed by this, because the force between the neighboring meshes cancel each other. In fact, the difference between the maximum pressure at the bow shock for the parameters used here and that for $D = \mu = Dp = 0$ was less than 10%.

6.2.2   Coordinate system and boundary conditions

A quarter simulation box for $x_1 \leq x \leq x_0$, $0 \leq y \leq y_0$, and $0 \leq z \leq z_0$ can be used in the Cartesian coordinate system in Figure 6.1, since we assume symmetry conditions which are consistent with the dipole magnetic field. The center of the earth is assumed to be located at $(x, y, z) = (0, 0, 0)$, and the solar wind is assumed to flow into the box in the x direction through the boundary at $x = x_0$. Therefore the following boundary conditions are imposed for each physical quantity, $\phi = (\rho, \mathbf{v}, p, \mathbf{B})$: (1) fixed boundary $\phi = $ const at $x = x_0$; (2) free boundary $\partial \phi/\partial x = 0$ at $x = x_1$; (3) free boundary at an angle of 45° to the x axis, $\partial \phi/\partial y = 0$ at $y = y_0$, $\partial \phi/\partial z = 0$ at $z = z_0$; (4) mirror boundary at $z = 0$,
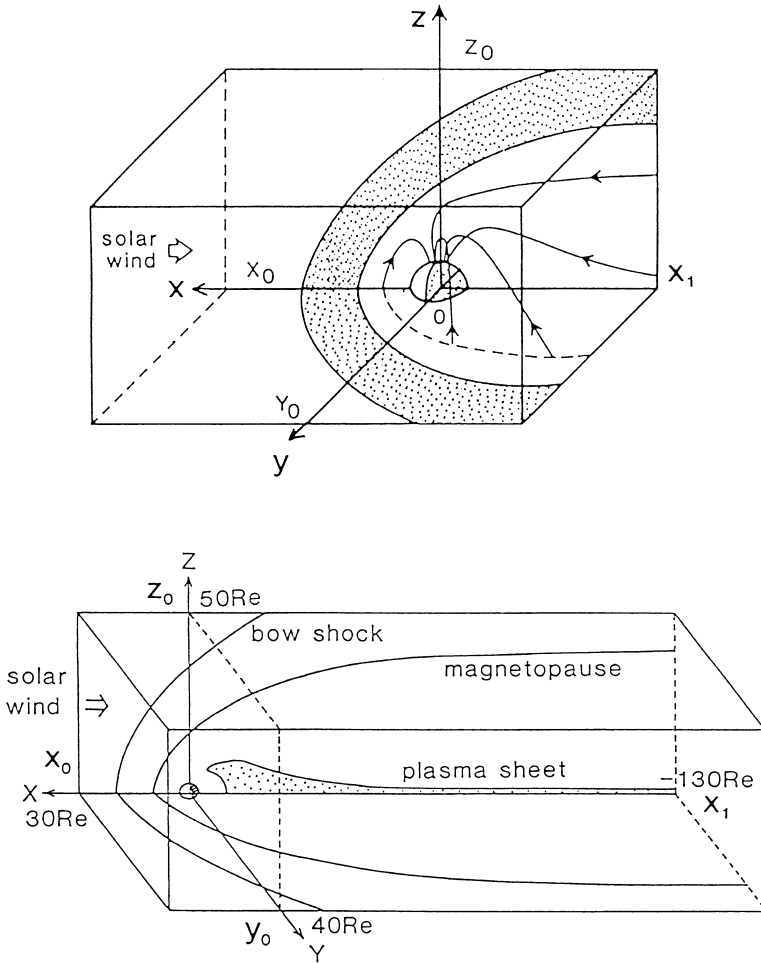
Figure 6.1: Solar-magnetospheric coordinate system in the 3-dimensional global MHD simulation of the interaction of the solar wind with the earth's magnetosphere (upper panel) and the schematic diagram of the magnetosphere with a long magnetotail region (lower panel).

$$\frac{\partial \rho}{\partial z} = \frac{\partial p}{\partial z} = \frac{\partial v_x}{\partial z} = \frac{\partial v_y}{\partial z} = \frac{\partial B_z}{\partial z} = 0 \qquad (6.6)$$

$$v_z = B_x = B_y = 0 \qquad (6.7)$$

(5) mirror boundary at $y = 0$,

$$\frac{\partial \rho}{\partial y} = \frac{\partial p}{\partial y} = \frac{\partial v_x}{\partial y} = \frac{\partial v_z}{\partial y} = \frac{\partial B_x}{\partial y} = \frac{\partial B_z}{\partial y} = 0 \qquad (6.8)$$

$$v_y = B_y = 0 \qquad (6.9)$$

(6) all physical quantities are fixed for

$$\xi = (x^2 + y^2 + z^2)^{1/2} \leq \xi_a \quad (= 3.5) \qquad (6.10)$$

The internal quantity ϕ_{in} at the initial state and the external quantity ϕ_{ex} are at each time step connected by the introduction of a smooth function $f \equiv a_0 h^2 (a_0 h^2 + 1)$ as

$$\phi = f\phi_{ex} + (1 - f)\phi_{in} \qquad (6.11)$$

where $a_0 = 100$, $h = (\xi/\xi_a)^2 - 1$ for $\xi \geq \xi_a$ and $h = 0$ for $\xi < \xi_a$.

A fresh solar wind always flows into the simulation box through the boundary accompanying the IMF and can interact with the dipole field of the earth. The state in the neighborhood of the earth does not vary from the initial state. The tail, upper, and side boundaries were cut at $x = x_1$, $z = z_0$, and $y = y_0$, where $x_0 = y_0 = z_0 = 48.8 R_E$ are typical parameters, and the free boundary condition, in which the spatial derivative for all the quantities is zero, was imposed. This boundary condition has less influence on the inside phenomena when the plasma flows outward through the boundary. We used it to minimize the effect of this boundary condition in our initial value problem.

6.2.3   Initial conditions

A steady state ionosphere is used in the neighborhood of the earth. The plasma number density is approximately proportional to the magnitude of the magnetic field, and the temperature is proportional to the radial distance for $1 \leq \xi \leq 6$. Thus the following initial conditions are used for the ionosphere near the earth:

Density

$$\begin{aligned} \rho_0 &= \xi^{-3} & \rho_0 &\geq 0.2\rho_{sw} \\ \rho_0 &= 0.2\rho_{sw} & \rho_0 &< 0.2\rho_{sw} \end{aligned} \qquad (6.12)$$

Plasma pressure

$$\begin{aligned} p_0 &= p_{00}\xi^{-2} & p_0 &\geq p_{sw} \\ p_0 &= p_{sw} & p_0 &< p_{sw} \end{aligned} \qquad (6.13)$$

Gravity force

$$\mathbf{g} = -\frac{g_0}{\xi^3}(x, y, z) \tag{6.14}$$

Dipole magnetic field

$$\mathbf{B}_d = \frac{1}{\xi^5}(-3xz, \ -3yz, \ x^2 + y^2 - 2z^2) \tag{6.15}$$

where $g_0 = 1.35 \times 10^{-6}$ and $p_{00} = (\gamma - 1)g_0/\gamma = 5.4 \times 10^{-7}$.

The solar wind parameters used are $\rho_{sw} = 5 \times 10^{-4}$ (corresponding to 5/cm^3), $\mathbf{v}_{sw} = (v_{sw}, 0, 0)$ at $x = -x_0$, $v_{sw} = 0.0441 - 0.118$ (300-800 km/s), $p_{sw} = 3.56 \times 10^{-8}$ ($T_{sw} = 2 \times 10^5$ K), and $B_{IMF} = 0$ or $\pm 1.5 \times 10^{-4}(\pm 5$ nT), where B_{IMF} stands for the z component of the uniform IMF traveling with the solar wind.

The normalized equations in (6.1 – 6.5) are solved as an initial value problem under the boundary conditions by the two-step Lax-Wendroff method in order to obtain quasi-steady-state magnetospheric configuration. The mesh numbers of the calculation are for example $(N_x, N_y, N_z) = (60, 30, 30)$ plus the boundary mesh points. The mesh size is $\Delta x = \Delta y = \Delta z = 1.6$, and the time step Δt is chosen to be $3\Delta x/2 = 2.2s$ from the numerical stability condition of the difference scheme, $V_A^{max}\Delta t < (1/2)\Delta x$, where $V_A^{max}(= \xi_a^{-3/2})$ is the maximum Alfvén velocity in the calculation domain.

6.3   Description of 2-Dimensional MHD Code

The 2-dimensional MHD simulation code which we will use in the present tutorial course is described in detail in comparison with the 3-dimensional global model in the previous section. The present purpose is to study the effects of the north-south component of the IMF to the magnetospheric configuration from a 2-dimensional global MHD simulation. Therefore, we try to solve the MHD and Maxwell's equations in the northern half plane as an initial value problem by using the two-step Lax-Wendroff scheme.

6.3.1   2-dimensional case of basic equations

The MHD and Maxwell's equations are solved as an initial value problem by using the two-step Lax-Wendroff scheme when all the physical quantities are assumed to be constant in the y-direction. The normalized MHD equations in (6.1 6.5) are rewritten separately by the following set of component equations in the x, y, z coordinates.

$$\frac{\partial \rho}{\partial t} = -\frac{\partial}{\partial x}V_x\rho - \frac{\partial}{\partial y}V_y\rho - \frac{\partial}{\partial z}V_z\rho + D\left\{\frac{\partial^2}{\partial x^2} + \frac{\partial^2}{\partial y^2} + \frac{\partial^2}{\partial z^2}\right\}\rho \tag{6.16}$$

$$\frac{\partial V_x}{\partial t} = -\left(V_x\frac{\partial}{\partial x} + V_y\frac{\partial}{\partial y} + V_z\frac{\partial}{\partial z}\right)V_x - \frac{1}{\rho}\frac{\partial P}{\partial x} + \frac{1}{\rho}\left(J_y B_z - J_z B_y\right)$$

$$+g_x + \frac{\mu\left(\frac{\partial^2}{\partial x^2} + \frac{\partial^2}{\partial y^2} + \frac{\partial^2}{\partial z^2}\right)V_x}{\rho} \qquad (6.17)$$

$$\frac{\partial V_y}{\partial t} = -\left(V_x\frac{\partial}{\partial x} + V_y\frac{\partial}{\partial y} + V_z\frac{\partial}{\partial z}\right)V_y - \frac{1}{\rho}\frac{\partial P}{\partial y} + \frac{1}{\rho}\left(J_z B_x - J_x B_z\right)$$

$$+g_y + \frac{\mu\left(\frac{\partial^2}{\partial x^2} + \frac{\partial^2}{\partial y^2} + \frac{\partial^2}{\partial z^2}\right)V_y}{\rho} \qquad (6.18)$$

$$\frac{\partial V_z}{\partial t} = -\left(V_x\frac{\partial}{\partial x} + V_y\frac{\partial}{\partial y} + V_z\frac{\partial}{\partial z}\right)V_z - \frac{1}{\rho}\frac{\partial P}{\partial z} + \frac{1}{\rho}\left(J_x B_y - J_y B_x\right)$$

$$+g_z + \frac{\mu\left(\frac{\partial^2}{\partial x^2} + \frac{\partial^2}{\partial y^2} + \frac{\partial^2}{\partial z^2}\right)V_z}{\rho} \qquad (6.19)$$

$$\frac{\partial P}{\partial t} = -\left(V_x\frac{\partial}{\partial x} + V_y\frac{\partial}{\partial y} + V_z\frac{\partial}{\partial z}\right)P - \gamma P\left(\frac{\partial}{\partial x}V_x + \frac{\partial}{\partial y}V_y + \frac{\partial}{\partial z}V_z\right)$$

$$+D_P\left(\frac{\partial^2}{\partial x^2} + \frac{\partial^2}{\partial y^2} + \frac{\partial^2}{\partial z^2}\right)P$$

$$(6.20)$$

$$\frac{\partial B_x}{\partial t} = \frac{\partial}{\partial y}\left(V_x B_y - V_y B_x\right) - \frac{\partial}{\partial z}\left(V_z B_x - V_x B_z\right)$$

$$+\eta\left(\frac{\partial^2}{\partial x^2} + \frac{\partial^2}{\partial y^2} + \frac{\partial^2}{\partial z^2}\right)B_x \qquad (6.21)$$

$$\frac{\partial B_y}{\partial t} = \frac{\partial}{\partial z}\left(V_y B_z - V_z B_y\right) - \frac{\partial}{\partial x}\left(V_x B_y - V_y B_x\right)$$

$$+\eta\left(\frac{\partial^2}{\partial x^2} + \frac{\partial^2}{\partial y^2} + \frac{\partial^2}{\partial z^2}\right)B_y \qquad (6.22)$$

$$\frac{\partial B_z}{\partial t} = \frac{\partial}{\partial x}\left(V_z B_x - V_x B_z\right) - \frac{\partial}{\partial y}\left(V_y B_z - V_z B_y\right)$$

$$+\eta\left(\frac{\partial^2}{\partial x^2} + \frac{\partial^2}{\partial y^2} + \frac{\partial^2}{\partial z^2}\right)B_z$$

$$(6.23)$$

In the 2-dimensional case, V_y, B_y and the derivative with respect to the y-component are always zero in (6.16 – 6.23) because the physical quantities are assumed to be uniform in the y-direction. Thus the 2-dimensional equations are trivial from (6.16-6.23) and we need to solve 6 arguments of $(\rho, V_x, V_z, P, B_x, B_z)$ from 8 arguments of the original MHD equations.

Though many parameters are same as in the 3-dimensional case described in the previous section, a few parameters should be changed due to the 2-dimension. The ratio of specific heats, $\gamma = 2$ due to the degree of freedom and $\mathbf{B}_d$ is replaced with the line dipole magnetic field. Typical numerical values are $\eta_0 = 0.01$ and $\mu/\rho_{sw} = 0.005$, and the typical magnetic Reynolds number becomes large as $S = \tau_\eta/\tau_A = 200 - 2000$. Moreover, the normalization quantities are exactly same.

6.3.2   Coordinate system and boundary conditions

A upper half simulation plane for $x_1 \leq x \leq x_0$, $0 \leq y \leq y_0$, and $0 \leq z \leq z_0$ can be used in the Cartesian coordinate system in Figure 6.2, since we assume symmetry conditions which are consistent with the line dipole magnetic field. The center of the earth is assumed to be located at $(x, z) = (0, 0)$, and the solar wind is assumed to flow into the simulation plane in the x direction through the boundary at $x = x_0$. Therefore the following boundary conditions are imposed for each physical quantity, $\phi = (\rho, \mathbf{v}, p, \mathbf{B})$: (1) fixed boundary $\phi = \text{const}$ at $x = x_0$; (2) free boundary $\partial\phi/\partial x = 0$ at $x = x_0$; (3) mirror boundary at $z = 0$,

$$\frac{\partial \rho}{\partial z} = \frac{\partial p}{\partial z} = \frac{\partial v_x}{\partial z} = \frac{\partial B_z}{\partial z} = 0 \tag{6.24}$$

$$v_z = B_x = 0 \tag{6.25}$$

(6) all physical quantities are fixed for

$$\xi = (x^2 + z^2)^{1/2} \leq \xi_a \ (= 16.0) \tag{6.26}$$

The internal quantity ϕ_{in} at the initial state and the external quantity ϕ_{ex} are at each time step connected by the introduction of a smooth function $f \equiv a_0 h^2 (a_0 h^2 + 1)$ as

$$\phi = f\phi_{ex} + (1 - f)\phi_{in} \tag{6.27}$$

where $a_0 = 100$, $h = (\xi/\xi_a)^2 - 1$ for $\xi \geq \xi_a$ and $h = 0$ for $\xi < \xi_a$.

A fresh solar wind always flows into the simulation plane through the boundary accompanying the IMF and can interact with the dipole field of the earth. The state in the neighborhood of the earth does not vary from the initial state. The tail, upper, and side boundaries were cut at $x = x_1$, $z = z_0$, and $y = y_0$, where $x_0 = y_0 = z_0 = 102 \, \text{R}_E$, and the free boundary condition, in which spatial derivative for all the quantities is zero, was imposed.
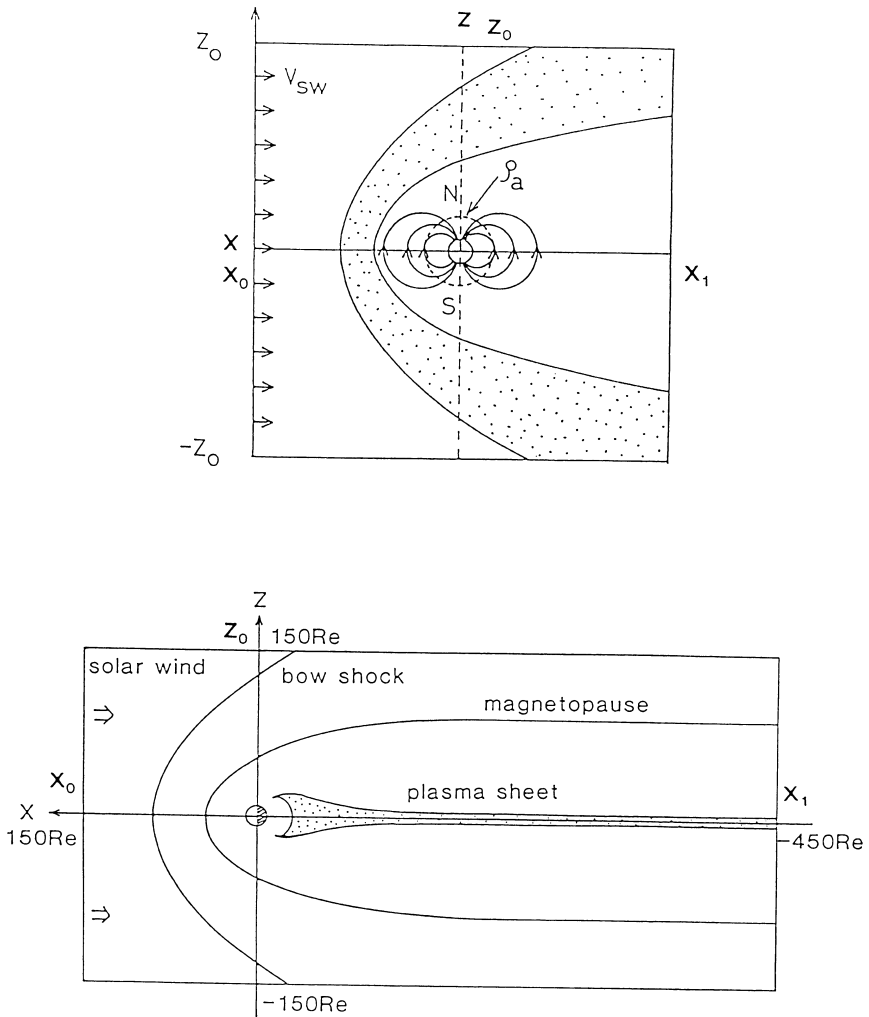
Figure 6.2: Solar-magnetospheric coordinate system in the 2-dimensional global MHD simulation of the interaction of the solar wind with the earth's magnetosphere (upper panel) and the schematic diagram of the magnetosphere with a long magnetotail region (lower panel).

6.3.3   Initial conditions

A steady state ionosphere is used in the neighborhood of the earth and the dependence on radial distance differs from that in 3-dimensional case. The plasma number density is proportional to the magnitude of the magnetic field, and the temperature is proportional to the radial distance for $1 \leq \xi \leq 30$. Thus the following initial ionospheric conditions are introduced near the earth in the 2-dimensional case:

Density

$$
\begin{aligned}
\rho_0 &= \xi^{-2} & \rho_0 &\geq 0.2\rho_{sw} \\
\rho_0 &= 0.2\rho_{sw} & \rho_0 &< 0.2\rho_{sw}
\end{aligned}
\tag{6.28}
$$

Plasma pressure

$$
\begin{aligned}
p_0 &= p_{00}\xi^{-1} & p_0 &\geq p_{sw} \\
p_0 &= p_{sw} & p_0 &< p_{sw}
\end{aligned}
\tag{6.29}
$$

Gravity force

$$
\mathbf{g} = -\frac{g_0}{\xi^2}(x, \ y, \ z)
\tag{6.30}
$$

Line dipole magnetic field

$$
\mathbf{B}_d = \frac{1}{\xi^4}(-2xz, \ x^2 - z^2)
\tag{6.31}
$$

where $g_0 = 1.35 \times 10^{-6}$ and $p_{00} = (\gamma - 1)g_0/\gamma = 6.8 \times 10^{-7}$.

When an image dipole field, Bid is put on $x = 2x_d$, x in (6.31) is only replaced with $x - 2x_d$. Therefore, the x-component of magnetic field is zero at $x = x_d$. Addition of the image dipole field corresponds to introduction of the Chapman-Ferraro type closed magnetosphere. The solar wind parameters are same as in Section 6.2.

The normalized equations in (6.16–6.23) are solved as an initial value problem under the boundary conditions by the two-step Lax-Wendroff method in order to obtain a 2-dimensional quasi-steady state magnetospheric configuration depending on the IMF z-component. The mesh numbers of the calculation are for example $(N_x, N_z) = (100, 50)$ plus the boundary mesh points. The mesh size is $\Delta x = \Delta z = 2.0$, and the time step Δt is chosen to be $8\Delta x/2 = 15s$ from the numerical stability condition of the difference scheme, $V_A^{max}\Delta t < (1/2)\Delta x$, where $V_A^{max}(= \xi_a^{-1})$ is the maximum Alfvén velocity in the calculation domain.

6.3.4   Application of two-step Lax-Wendroff method

Let us start to make a 2-dimensional MHD code by using the two-step Lax-Wendroff method. For example, equation (6.16) can be rewritten as

$$
\frac{\partial \rho}{\partial t} = -\frac{\partial}{\partial x}V_x\rho - \frac{\partial}{\partial y}V_y\rho
\tag{6.32}
$$

in the 2-dimension when the diffusion term is neglected. Thus we can introduce the following simple equation with the same format in order to apply the numerical scheme.

$$\frac{\partial F}{\partial t} = -\frac{\partial}{\partial x}F - \frac{\partial}{\partial y}F - F \tag{6.33}$$

The expression of difference scheme in the two-step Lax-Wendroff method is written by the next two steps.

(1) First step

$$F^t_{i+\frac{1}{2},j+\frac{1}{2}} = \frac{1}{4}\left(F^t_{i,j} + F^t_{i+1,j} + F^t_{i,j+1} + F^t_{i+1,j+1}\right) \tag{6.34}$$

$$\begin{aligned}
F^{t+\frac{1}{2}}_{i+\frac{1}{2},j+\frac{1}{2}} &= F^t_{i+\frac{1}{2},j+\frac{1}{2}} - \frac{1}{2}\Delta t F^t_{i+\frac{1}{2},j+\frac{1}{2}}\\
&- \frac{\Delta t}{4\Delta x}\left(F^t_{i+1,j+1} + F^t_{i+1,j} - F^t_{i,j+1} - F^t_{i,j}\right)\\
&- \frac{\Delta t}{4\Delta y}\left(F^t_{i+1,j+1} + F^t_{i,j+1} - F^t_{i+1,j} - F^t_{i,j}\right)
\end{aligned} \tag{6.35}$$

(2) Second step

$$\begin{aligned}
F^{t+\frac{1}{2}}_{i,j} &= \frac{1}{4}\left(F^{t+\frac{1}{2}}_{i-\frac{1}{2},j-\frac{1}{2}} + F^{t+\frac{1}{2}}_{i+\frac{1}{2},j-\frac{1}{2}} + F^{t+\frac{1}{2}}_{i-\frac{1}{2},j+\frac{1}{2}} + F^{t+\frac{1}{2}}_{i+\frac{1}{2},j+\frac{1}{2}}\right) \tag{6.36}\\
F^{t+1}_{i,j} &= F^t_{i,j} - \Delta t F^{t+\frac{1}{2}}_{i,j}\\
&- \frac{\Delta t}{2\Delta x}\left(F^{t+\frac{1}{2}}_{i+\frac{1}{2},j+\frac{1}{2}} + F^{t+\frac{1}{2}}_{i+\frac{1}{2},j-\frac{1}{2}} - F^{t+\frac{1}{2}}_{i-\frac{1}{2},j+\frac{1}{2}} - F^{t+\frac{1}{2}}_{i-\frac{1}{2},j-\frac{1}{2}}\right)\\
&- \frac{\Delta t}{2\Delta y}\left(F^{t+12}_{i+12,j+12} + F^{t+12}_{i-12,j+12} - F^{t+12}_{i+12,j-12} - F^{t+12}_{i-12,j-12}\right) \tag{6.37}
\end{aligned}$$

Here we use an abbreviation in a form of $F^t_{i,j} = F(t, x_i, y_j)$ and the spatial grids, Δx, Δy and the time step, Δt are introduced. That is, $t+1$, $i+1$, $j+1$ mean $t + \Delta t$, $x_i + \Delta x$, $y_j + \Delta y$, respectively.

For the first time we assume that $F^t_{i,j}$ is given for $2 \leq i \leq nx+1$ and $2 \leq j \leq ny+1$. Then $F^t_{i,j}$ at the boundary should be determined from the assumption of boundary condition. Using the two-step procedure, we can calculate new value of $F^{t+1}_{i,j}$. A temporally forward difference is used in the first step, on the other hand the time central difference is adopted in the second step.

The procedure of two-step Lax-Wendroff method is as follows;

1. $F(i, j)$ is given for $2 \leq i \leq nx1$ and $2 \leq j \leq ny1$

2. $F(i, j)$ for i=1,nx2 and j=1,ny2 is determined from boundary condition

3. 1st interpolation from (6.34)
$P(i,j) = \frac{1}{4}(F(i,j) + F(i+1,j) + F(i,j+1) + F(i+1,j+1))$
$U(i,j) = P(i,j)$

4. Calculation of 1st step from (6.35)

$$
\begin{aligned}
U(i,j) \;=\; & U(i,j) - \frac{1}{2}\Delta t P(i,j) \\
& - \frac{\Delta t}{4\Delta x}\left(F(i+1,j+1) + F(i+1,j) - F(i,j+1) - F(i,j)\right) \\
& - \frac{\Delta t}{4\Delta y}\left(F(i+1,j+1) + F(i,j+1) - F(i+1,j) - F(i,j)\right)
\end{aligned}
$$

$$(6.38)$$

5. 2nd interpolation from (6.36)
$P(i,j) = \frac{1}{4}(U(i-1,j-1) + U(i,j-1) + U(i-1,j) + U(i,j))$

6. Calculation of 2nd step from (6.37)

$$
\begin{aligned}
F(i,j) \;=\; & F(i,j) - \Delta t P(i,j) \\
& - \frac{\Delta t}{2\Delta x}\left(U(i,j) + U(i,j-1) - U(i-1,j) - U(i-1,j-1)\right) \\
& - \frac{\Delta t}{2\Delta y}\left(U(i,j) + U(i-1,j) - U(i,j-1) - U(i-1,j-1)\right)
\end{aligned}
$$

$$(6.39)$$

As the result of these sequences, $F(i,j)$ in a time step advance is calculated, where $nx1 = nx+1, nx2 = nx+2, ny1 = ny+1, ny2 = ny+2$. In the simulation code we use one dimensional array to keep a faster computation. The relation between the one dimensional argument $F(i1)$ and the two dimensional array argument $F(i,j)$ is

$$F(i1) = F(i,j) \quad \text{for} \;\; i1 = i + nx2 * (j-1)$$

The schematic diagram of the procedure of the two-step Lax-Wendroff method is shown in Figures 6.3 and 6.4. If one wants to directly apply the two step Lax-Wendroff method to (6.16), we can obtain the following difference expressions for the 3-dimensional case.
    Modified two-step Lax-Wendroff method in 3-dimension
(1) First step

$$
\begin{aligned}
\rho^t_{i+\frac{1}{2},j+\frac{1}{2},k+\frac{1}{2}} = \frac{1}{8}\Big(& \rho^t_{i,j,k} + \rho^t_{i+1,j,k} + \rho^t_{i,j+1,k} + \rho^t_{i,j,k+1} \\
& + \rho^t_{i+1,j+1,k} + \rho^t_{i+1,j,k+1} + \rho^t_{i,j+1,k+1} + \rho^t_{i+1,j+1,k+1}\Big)
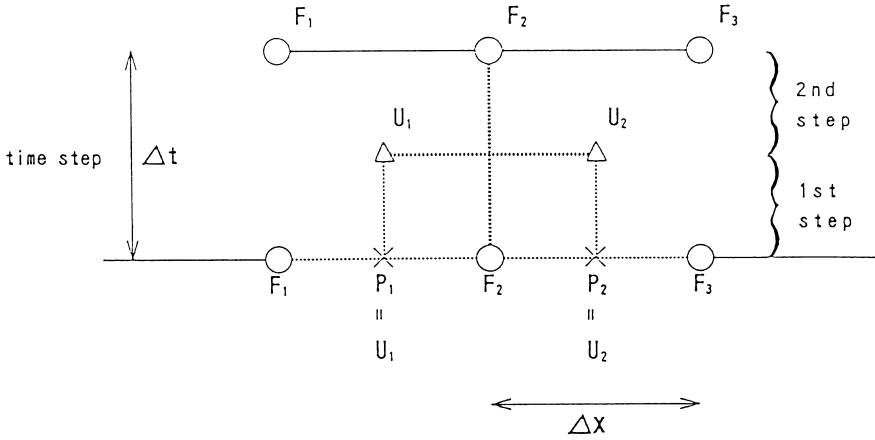\end{aligned}
$$

$$(6.40)$$

Figure 6.3: Schematic diagram on the numerical procedure of the two-step Lax-Wendroff method in the one dimensional space.
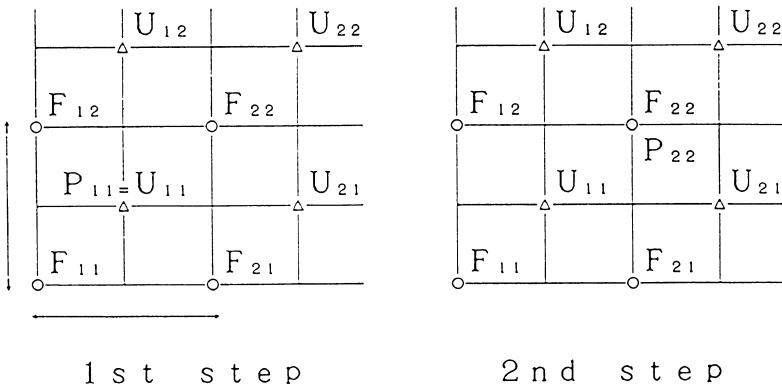
Figure 6.4: Schematic diagram on the grid connection of the two-step Lax-Wendroff method in the two dimensional case.

$$
\begin{aligned}
\rho^{t+\frac{1}{2}}_{i+\frac{1}{2},j+\frac{1}{2},k+\frac{1}{2}} = {} & \rho^{t}_{i+\frac{1}{2},j+\frac{1}{2},k+\frac{1}{2}} \\
& -\frac{\Delta t}{8\Delta x}\Big\{(\rho V_x)^{t}_{i+1,j+1,k+1} + (\rho V_x)^{t}_{i+1,j+1,k} + (\rho V_x)^{t}_{i+1,j,k+1} + (\rho V_x)^{t}_{i+1,j,k} \\
& \qquad\qquad - (\rho V_x)^{t}_{i,j+1,k+1} - (\rho V_x)^{t}_{i,j+1,k} - (\rho V_x)^{t}_{i,j,k+1} - (\rho V_x)^{t}_{i,j,k}\Big\} \\
& -\frac{\Delta t}{8\Delta y}\Big\{(\rho V_y)^{t}_{i+1,j+1,k+1} + (\rho V_y)^{t}_{i+1,j+1,k} + (\rho V_y)^{t}_{i,j+1,k+1} + (\rho V_y)^{t}_{i,j+1,k} \\
& \qquad\qquad - (\rho V_y)^{t}_{i+1,j,k+1} - (\rho V_y)^{t}_{i+1,j,k} - (\rho V_y)^{t}_{i,j,k+1} - (\rho V_y)^{t}_{i,j,k}\Big\} \\
& -\frac{\Delta t}{8\Delta z}\Big\{(\rho V_z)^{t}_{i+1,j+1,k+1} + (\rho V_z)^{t}_{i+1,j,k+1} + (\rho V_z)^{t}_{i,j+1,k+1} + (\rho V_z)^{t}_{i,j,k+1} \\
& \qquad\qquad - (\rho V_z)^{t}_{i+1,j+1,k} - (\rho V_z)^{t}_{i+1,j,k} - (\rho V_z)^{t}_{i,j+1,k} - (\rho V_z)^{t}_{i,j,k}\Big\}
\end{aligned}
\tag{6.41}
$$

(2) Second step

$$
\begin{aligned}
\rho^{t+1}_{i,j,k} = {} & \rho^{t}_{i,j,k} \\
& -\frac{\Delta t}{4\Delta x}\Big\{(\rho V_x)^{t+\frac{1}{2}}_{i+\frac{1}{2},j+\frac{1}{2},k+\frac{1}{2}} + (\rho V_x)^{t+\frac{1}{2}}_{i+\frac{1}{2},j+\frac{1}{2},k-\frac{1}{2}} \\
& \qquad\quad + (\rho V_x)^{t+\frac{1}{2}}_{i+\frac{1}{2},j-\frac{1}{2},k+\frac{1}{2}} + (\rho V_x)^{t+\frac{1}{2}}_{i+\frac{1}{2},j-\frac{1}{2},k-\frac{1}{2}} \\
& \qquad\quad - (\rho V_x)^{t+\frac{1}{2}}_{i-\frac{1}{2},j+\frac{1}{2},k+\frac{1}{2}} - (\rho V_x)^{t+\frac{1}{2}}_{i-\frac{1}{2},j+\frac{1}{2},k-\frac{1}{2}} \\
& \qquad\quad - (\rho V_x)^{t+\frac{1}{2}}_{i-\frac{1}{2},j-\frac{1}{2},k+\frac{1}{2}} - (\rho V_x)^{t+\frac{1}{2}}_{i-\frac{1}{2},j-\frac{1}{2},k-\frac{1}{2}}\Big\} \\
& -\frac{\Delta t}{4\Delta y}\Big\{(\rho V_y)^{t+\frac{1}{2}}_{i+\frac{1}{2},j+\frac{1}{2},k+\frac{1}{2}} + (\rho V_y)^{t+\frac{1}{2}}_{i+\frac{1}{2},j+\frac{1}{2},k-\frac{1}{2}} \\
& \qquad\quad + (\rho V_y)^{t+\frac{1}{2}}_{i-\frac{1}{2},j+\frac{1}{2},k+\frac{1}{2}} + (\rho V_y)^{t+\frac{1}{2}}_{i-\frac{1}{2},j+\frac{1}{2},k-\frac{1}{2}} \\
& \qquad\quad - (\rho V_y)^{t+\frac{1}{2}}_{i+\frac{1}{2},j-\frac{1}{2},k+\frac{1}{2}} - (\rho V_y)^{t+\frac{1}{2}}_{i+\frac{1}{2},j-\frac{1}{2},k-\frac{1}{2}} \\
& \qquad\quad - (\rho V_y)^{t+\frac{1}{2}}_{i-\frac{1}{2},j-\frac{1}{2},k+\frac{1}{2}} - (\rho V_y)^{t+\frac{1}{2}}_{i-\frac{1}{2},j-\frac{1}{2},k-\frac{1}{2}}\Big\} \\
& -\frac{\Delta t}{4\Delta z}\Big\{(\rho V_z)^{t+\frac{1}{2}}_{i+\frac{1}{2},j+\frac{1}{2},k+\frac{1}{2}} + (\rho V_z)^{t+\frac{1}{2}}_{i+\frac{1}{2},j-\frac{1}{2},k+\frac{1}{2}} \\
& \qquad\quad + (\rho V_z)^{t+\frac{1}{2}}_{i-\frac{1}{2},j+\frac{1}{2},k+\frac{1}{2}} + (\rho V_z)^{t+\frac{1}{2}}_{i-\frac{1}{2},j-\frac{1}{2},k+\frac{1}{2}} \\
& \qquad\quad - (\rho V_z)^{t+\frac{1}{2}}_{i+\frac{1}{2},j+\frac{1}{2},k-\frac{1}{2}} - (\rho V_z)^{t+\frac{1}{2}}_{i+\frac{1}{2},j-\frac{1}{2},k-\frac{1}{2}} \\
& \qquad\quad - (\rho V_z)^{t+\frac{1}{2}}_{i-\frac{1}{2},j+\frac{1}{2},k-\frac{1}{2}} - (\rho V_z)^{t+\frac{1}{2}}_{i-\frac{1}{2},j-\frac{1}{2},k-\frac{1}{2}}\Big\} \\
& +\frac{\Delta t}{\Delta x^2}\Big\{\rho^{t}_{i+1,j+1,k+1} + \rho^{t}_{i+1,j+1,k} + \rho^{t}_{i+1,j,k+1} + \rho^{t}_{i+1,j,k}
\end{aligned}
$$

$$-2 \left(\rho^t_{i,j+1,k+1} + \rho^t_{i,j+1,k} + \rho^t_{i,j,k+1} + \rho^t_{i,j,k} \right)$$

$$+\rho^t_{i-1,j+1,k+1} + \rho^t_{i-1,j+1,k} + \rho^t_{i-1,j,k+1} + \rho^t_{i-1,j,k} \Big\}$$

$$+ \quad \frac{\Delta t}{\Delta y^2} \Big\{ \rho^t_{i+1,j+1,k+1} + \rho^t_{i+1,j+1,k} + \rho^t_{i,j+1,k+1} + \rho^t_{i,j+1,k}$$

$$-2 \left(\rho^t_{i+1,j,k+1} + \rho^t_{i+1,j,k} + \rho^t_{i,j,k+1} + \rho^t_{i,j,k} \right)$$

$$+\rho^t_{i+1,j-1,k+1} + \rho^t_{i+1,j-1,k} + \rho^t_{i,j-1,k+1} + \rho^t_{i,j-1,k} \Big\}$$

$$+ \quad \frac{\Delta t}{\Delta z^2} \Big\{ \rho^t_{i+1,j+1,k+1} + \rho^t_{i+1,j,k+1} + \rho^t_{i,j+1,k+1} + \rho^t_{i,j,k+1}$$

$$-2 \left(\rho^t_{i+1,j+1,k} + \rho^t_{i+1,j,k} + \rho^t_{i,j+1,k} + \rho^t_{i,j,k} \right)$$

$$+\rho^t_{i+1,j+1,k-1} + \rho^t_{i+1,j,k-1} + \rho^t_{i,j+1,k-1} + \rho^t_{i,j,k-1} \Big\} \qquad (6.42)$$

6.4   Execution of 2-Dimensional MHD Code

6.4.1   Set up of numerical parameters

Program name of the main MHD simulation code is RECTG81 and the 2-dimensional MHD code is set up to simulate the interaction between the solar wind and the earth's magnetosphere. However it is a typical MHD simulation code to be applied to other phenomena. The specific features to simulate the earth's magnetosphere just come from the inner boundary condition of ionosphere, the upstream boundary condition of solar wind, and the initial condition such as the initial distribution of magnetic field.

   The several important parameters in the present global simulation are as follows;

> Grid number $(N_x, N_z) = (100, 50)$
> Grid size $(\Delta x, \Delta z) = (2, 2)$
> Time step $\Delta t = \frac{1}{2}\Delta x \times THR = 8\Delta x = 16(= 15s)$
> IMF B_z component $B_z = 0, \pm 1.5 \ (\pm 5nT)$
> Speed of solar wind $V_{sw} = 0.044 \ (300km/s)$

Exercise in 2-dimensional MHD simulation

1. Change the magnitude of IMF B_z component.
   $B_z = \text{IBZ} = \text{CP}(11) = \pm 1.5 \ (\pm 5nT)$

2. Change the velocity or density of the solar wind
   $V_{sw} = CP(8) = 0.044 \ (300km/s)$
   $\rho = \text{RO01} = 5 \times 10^{-4} \ (5/cc)$

3. Change the magnitude of earth's dipole field
   $B_o = CJ(4) = 1.0$

4. Change the resistivity model
   $\eta = $ EAT

5. Change the initial magnetosphere
   subroutine EQUIP4   2-dimensional dipole model
   EQUIP5   image dipole model

6.4.2   Examples of execution

Examples of the 2-dimensional MHD simulation are shown in Figures 6.5 ∼ 6.8. Figure 6.5 shows the initial configuration of the simulation.   The upper left panel presents profiles of the physical quantities in the sun-earth line (in the x-axis), where B_z, V_x, ρ and P are seen from the top panel to the bottom panel. The upper right panel present profiles of the physical quantities in the north-south line (in the z-axis). B_z, V_x, ρ and P are also seen from the top panel to the bottom panel. The lower 9 panels show 2-dimensional magnetospheric patterns:

1. magnetic flux   (left bottom)

2. plasma pressure   (center bottom)

3. plasma density   (right bottom)

4. magnitude of magnetic flux

5. flow velocity

6. magnetic field

7. current density

8. vorticity, $\Omega = \nabla \times V$

9. electric field, E_y

6.4.3   Graphics output

In order to obtain graphics output we use a graphics program "RDSPF801" and a graphics subroutine package "SUBM2AS". In the graphics main program, GRAP7G is a subroutine to draw line for profile in the sun-earth line, GRPH1M is to draw the vector presentation and GRAP4M is to draw contour-line.
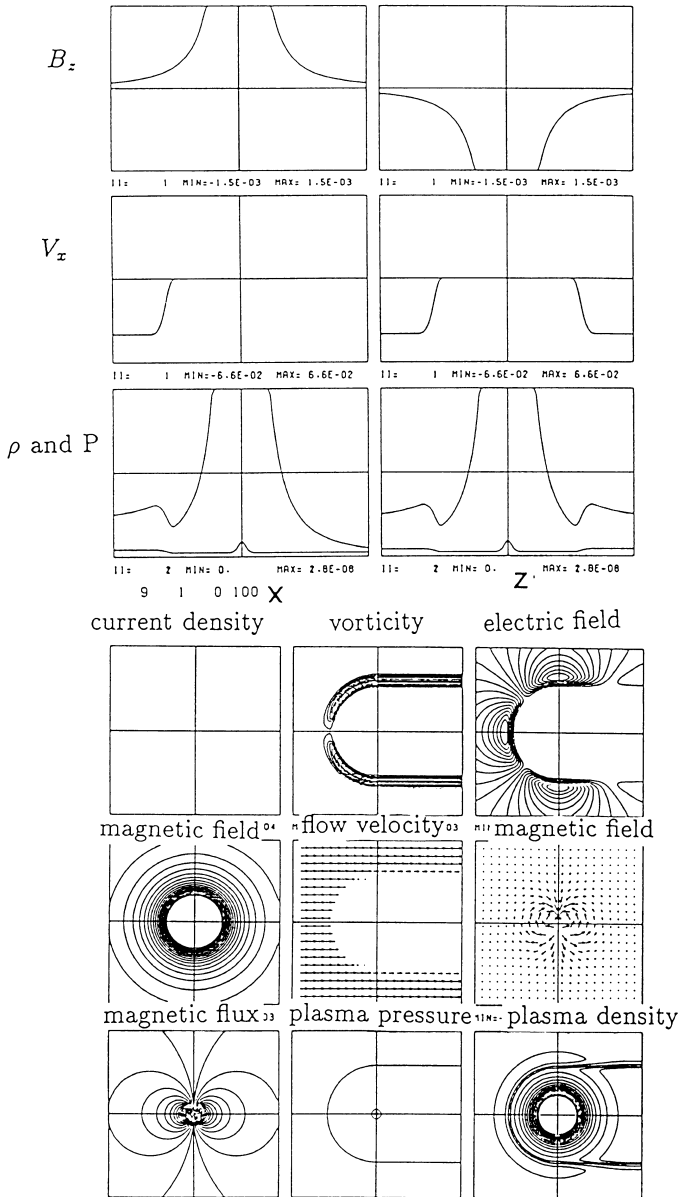
Figure 6.5: Initial state of the 2-dimensional global MHD simulation of interaction between the solar wind and the earth's magnetosphere. The top left panel shows profiles of physical quantities in the sun-earth line, the top right panel shows those in the north-south line (or z-axis) and the bottom shows two dimensional patterns.
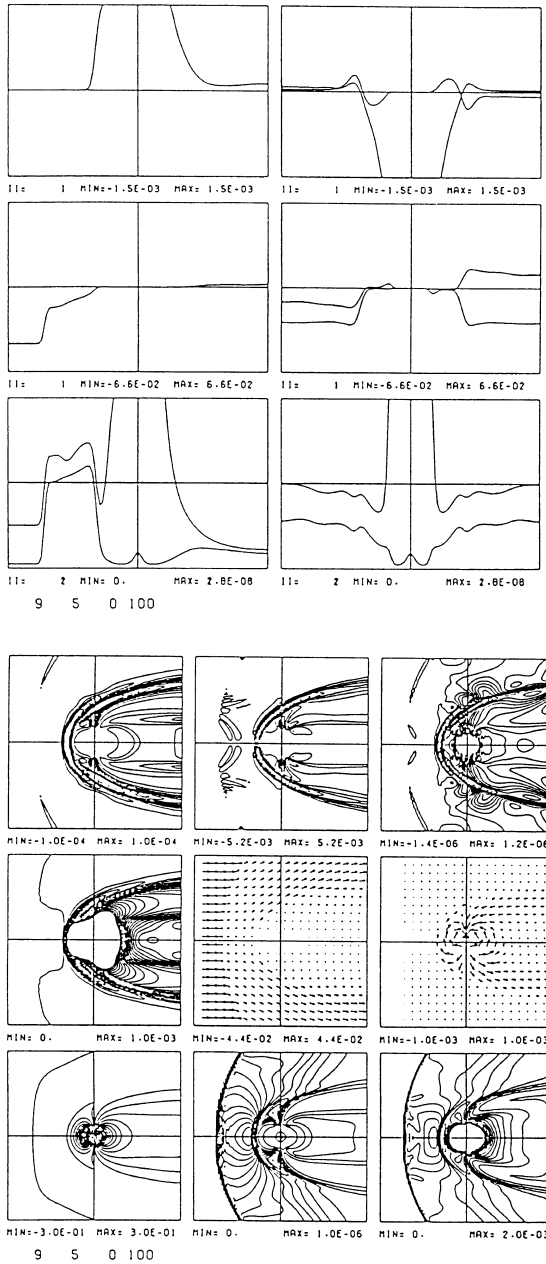
Figure 6.6: Quasi-steady state magnetospheric configuration in the 2-D MHD simulation for no uniform IMF ($B_{z0} = 0 nT$).
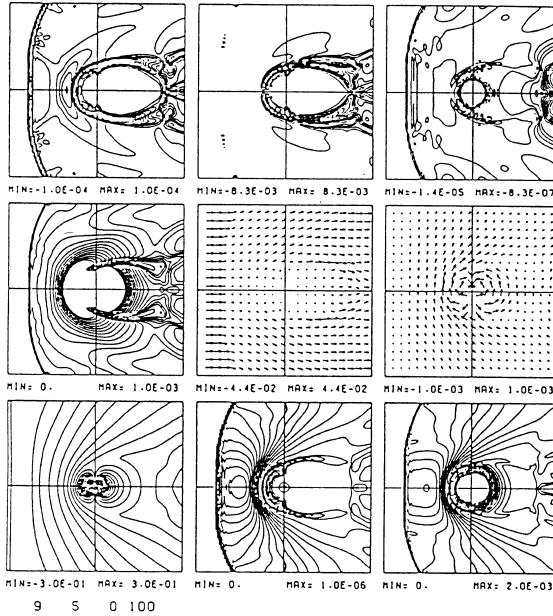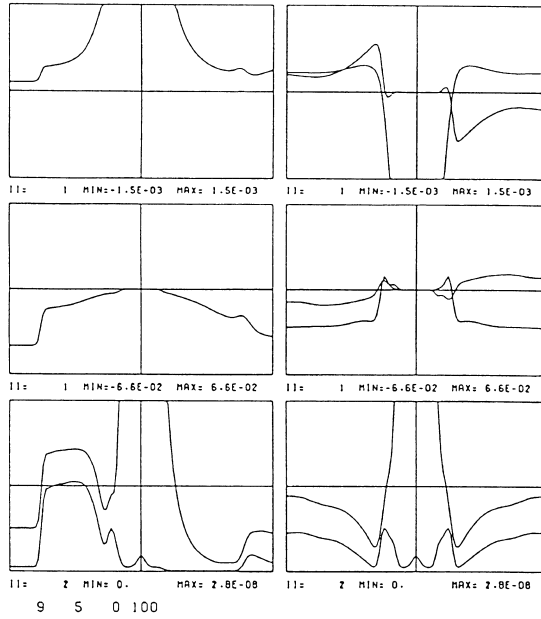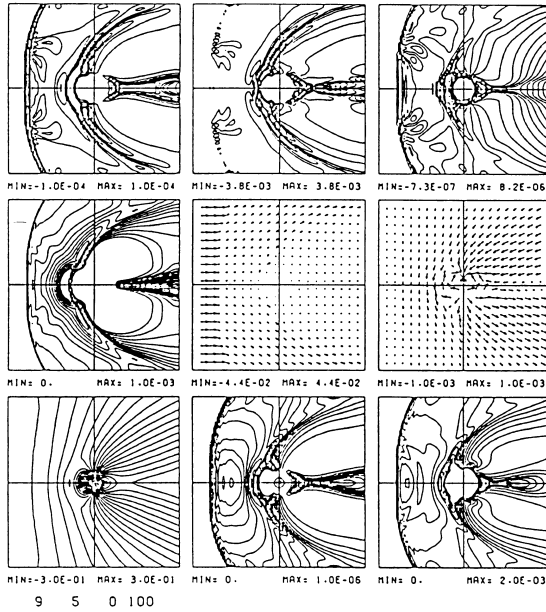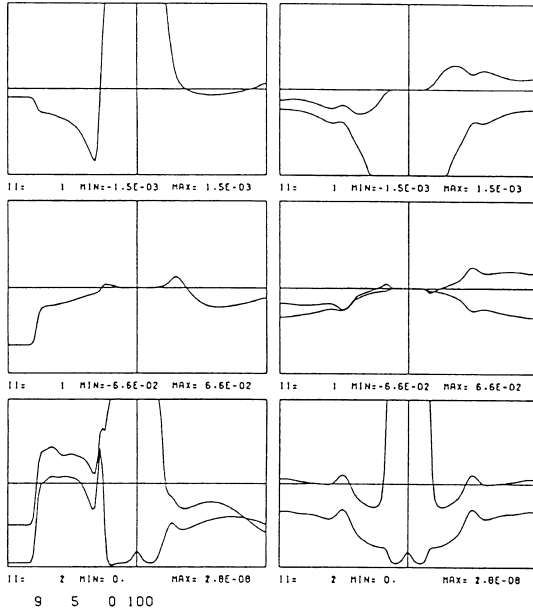
Figure 6.7: Quasi-steady state magnetospheric configuration in the 2-D MHD simulation for northward IMF ($B_{z0} = 5nT$).

Figure 6.8: Quasi-steady state magnetospheric configuration in the 2-D MHD simulation for southward IMF ($B_{z0} = -5nT$).

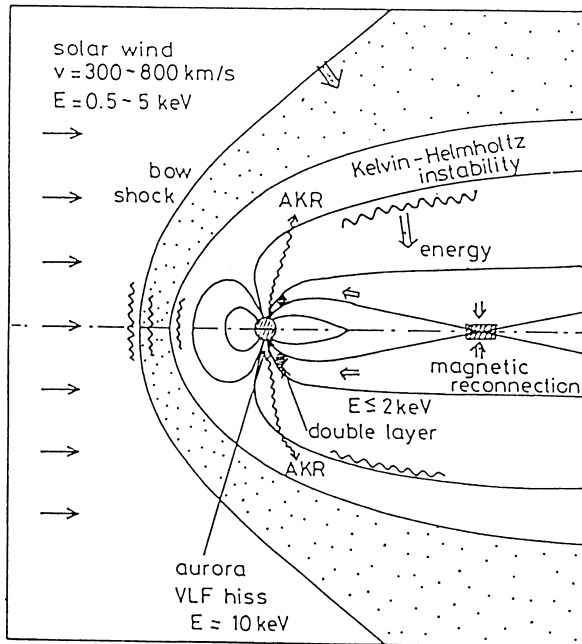Figure 6.9: Schematic diagram of the earth's magnetospheric phenomena.

6.5 MHD Simulation of Earth's Magnetosphere

6.5.1 2-dimensional simulation results

In this section several 2-dimensional MHD simulation results are demonstrated. In Figure 6.9, Schematic diagram of the earth's magnetospheric phenomena are displayed. From the MHD simulation we can study the global structure of magnetosphere and macroscopic instability such as Kelvin-Helmholtz instability at the magnetopause and magnetic reconnection at the dayside magnetopause and in the magnetotail. The MHD code handles the space plasma as single fluid. Therefore, phenomena in which particles play an important role are beyond its task.

In Figure 6.10, typically simulated magnetospheres depending on the IMF z-component are shown in the initial state and the quasi-steady state. The term of "quasi-steady state" means here that global structure of the magnetosphere does not change, however the structure of small scale at the magnetopause and in the plasma sheet still continues to change gradually.

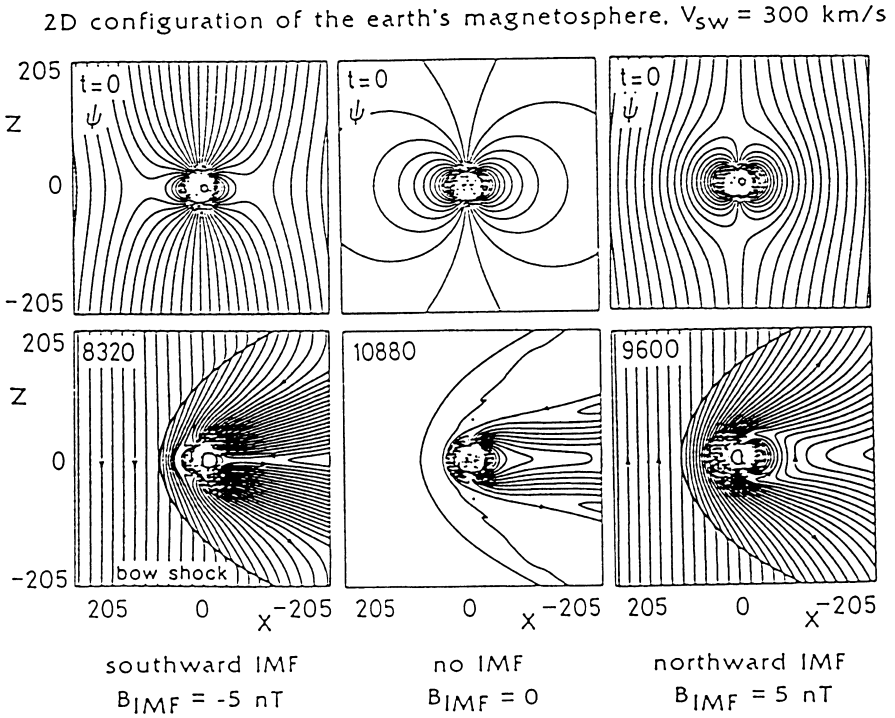In Figure 6.11 is shown 2-dimensional magnetosphere with a long magneto-

2D configuration of the earth's magnetosphere, V_{sw} = 300 km/s

Figure 6.10: Simulated 2-dimensional configurations of the earth's magneto-sphere in the initial state and the quasi-steady state, when the uniform IMF (southward, no or northward IMF) was imposed in the whole region at the initial time.

tail. The configuration does not change so much when time elapses. The grid number is (N_x, N_z)=(400, 100) and $\Delta x = \Delta z = 1.5Re$. The time evolution on formation of the 2-dimensional magnetosphere is shown in Figure 6.12, where $(N_x, N_z) = (400, 100)$ and $\Delta x = \Delta z = 1Re$: The behavior of draping of magnetic field lines is clearly seen and another interesting point is the formation of cusp which somewhat moves sunward.

6.5.2   3-dimensional simulation results

Two examples of 3-dimensional global simulation are shown in Figures 6.13 and 6.14. In Figure 6.13, the difference of configuration of magnetic field lines clearly tells the effect of the IMF z-component. In Figure 6.14, the structure of discontinuity composed of the bow shock and magnetopause can be compared each other when we choose a particular grid size Δx=1.6Re (top), Δx = 1.0(center) and $\Delta x = 0.5Re$ (bottom). From these global simulation, you can recognize how spatial resolution is important if we want to discuss the phenomena associated with the discontinuity.

6.5.3   High resolution MHD simulation

Recently we have tried to develop a higher resolution MHD simulation code "modified leap-frog method". In Figure 6.15 is shown the schematic diagram of computation procedure for the method. The modified leap-frog method is fundamentally a combination of the leap frog method and the two-step Lax-Wendroff method. We use two-step Lax-Wendroff method in the first 1 step and use the leap-frog method in the successive (l-1) time steps. Therefore, the advantage for leap-frog method is reasonably included. That is, numerical accuracy of phase velocity is greatly improved and the absolute value of amplification factor is also close unity (see Appendix: A and B).

We will discuss the amplification factor of the high resolurion MHD code in more detail.

The amplification factor of two-step Lax-Wendroff method is

$$A_{LW} \;\; = \;\; 1 - 2\delta^2 \sin^2 \frac{\kappa}{2} + i\delta \sin \kappa \tag{6.43}$$

$$|A_{LW}|^2 \;\; = \;\; 1 + 4(\delta^4 - \delta^2) \sin^4 \frac{\kappa}{2} \tag{6.44}$$

and that of leap-frog method is

$$A_{LF} \;\; = \;\; 1 - 2\delta^2 \sin^2 \frac{\kappa}{2} \pm i2\delta \sin \frac{\kappa}{2} (1 - \delta^2 \sin^2 \frac{\kappa}{2})^{\frac{1}{2}} \tag{6.45}$$
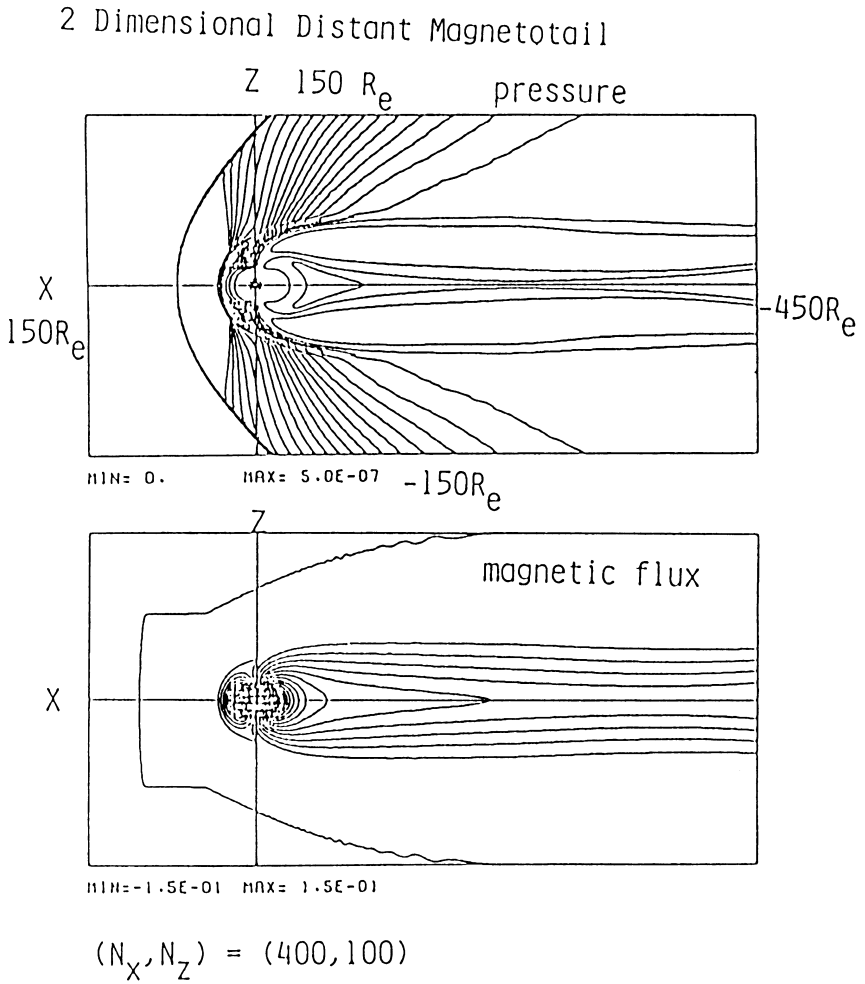
$$|A_{LF}| \;\; = \;\; 1 \tag{6.46}$$

2 Dimensional Distant Magnetotail

Figure 6.11: Simulated 2-dimensional magnetospheric configuration with a long magnetotail in almost steady state.

MIN=-1.5E-01   MAX= 1.5E-01

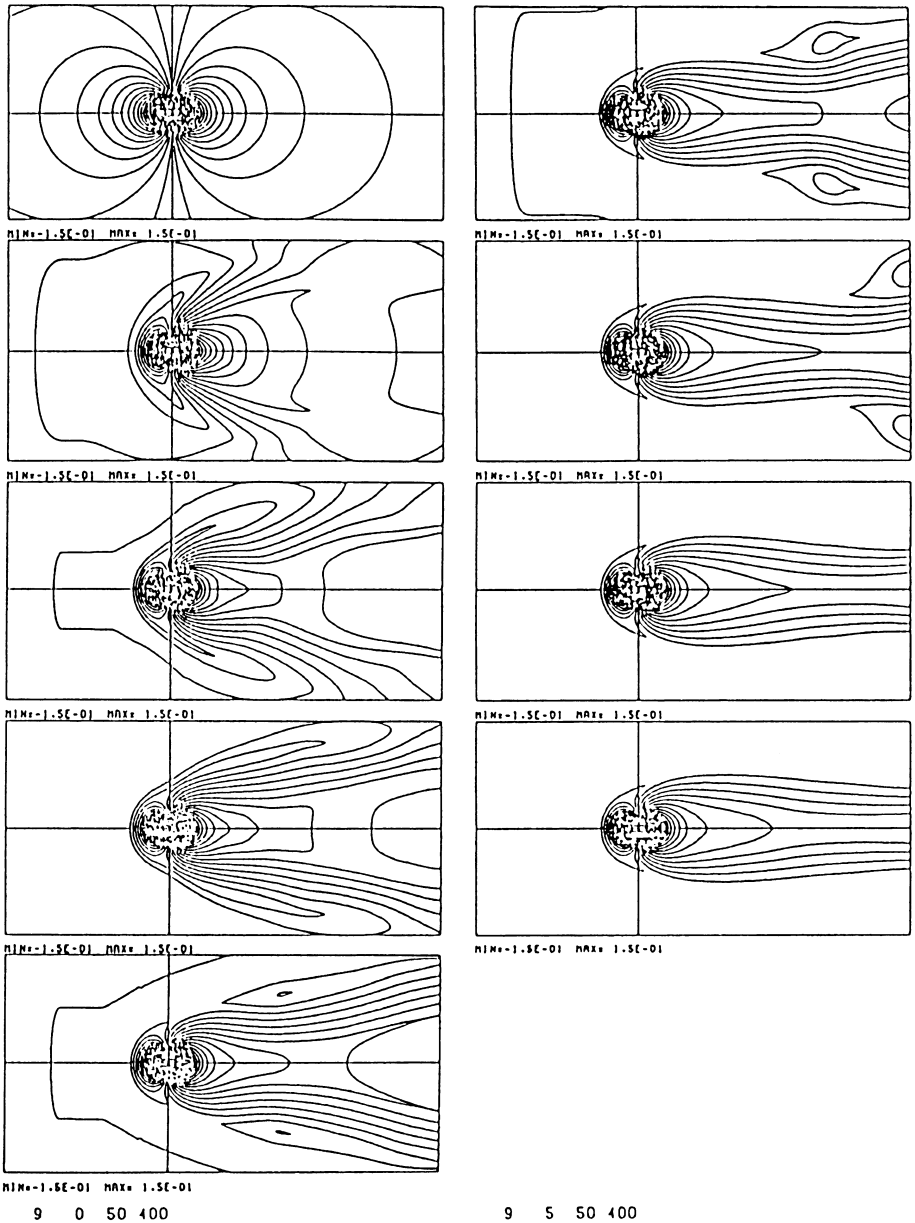9   0   50 400   9   5   50 400

Figure 6.12: Time evolution on formation of the 2-dimensional magnetospheric structure for no uniform IMF.

$B_z = -5$ nT

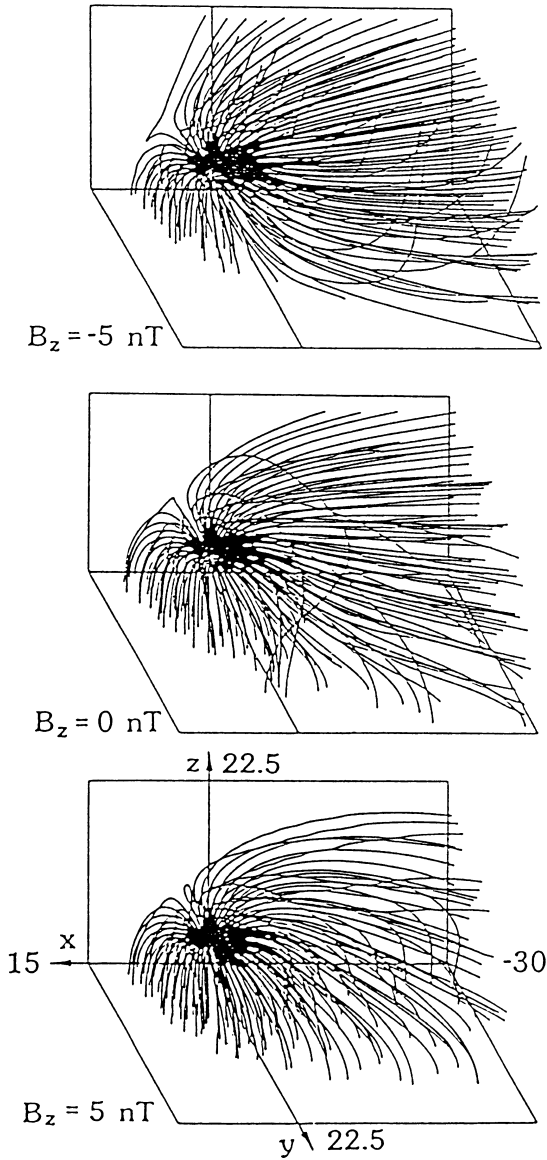$B_z = 0$ nT

z↓ 22.5

15 → x

-30

$B_z = 5$ nT

y↘ 22.5

Figure 6.13: Comparison of the simulated magnetospheres for northward, no uniform, and southward IMF conditions in 3-dimension.
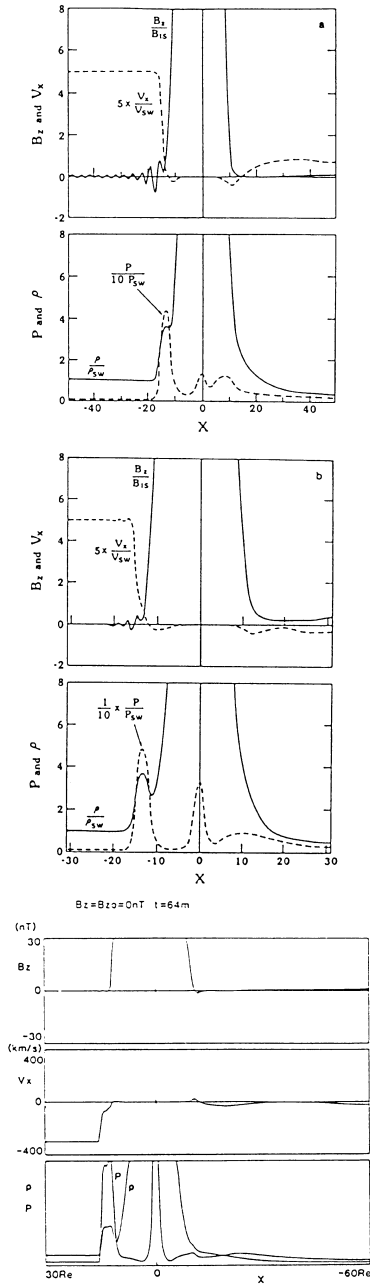
Figure 6.14: Comparison of the spatial resolution in the simulated 3-dimensional magnetosphere for (a) $\Delta x = 1.6Re$, (b) $\Delta x = 1.0Re$ and (c) $\Delta x = 0.5Re$.
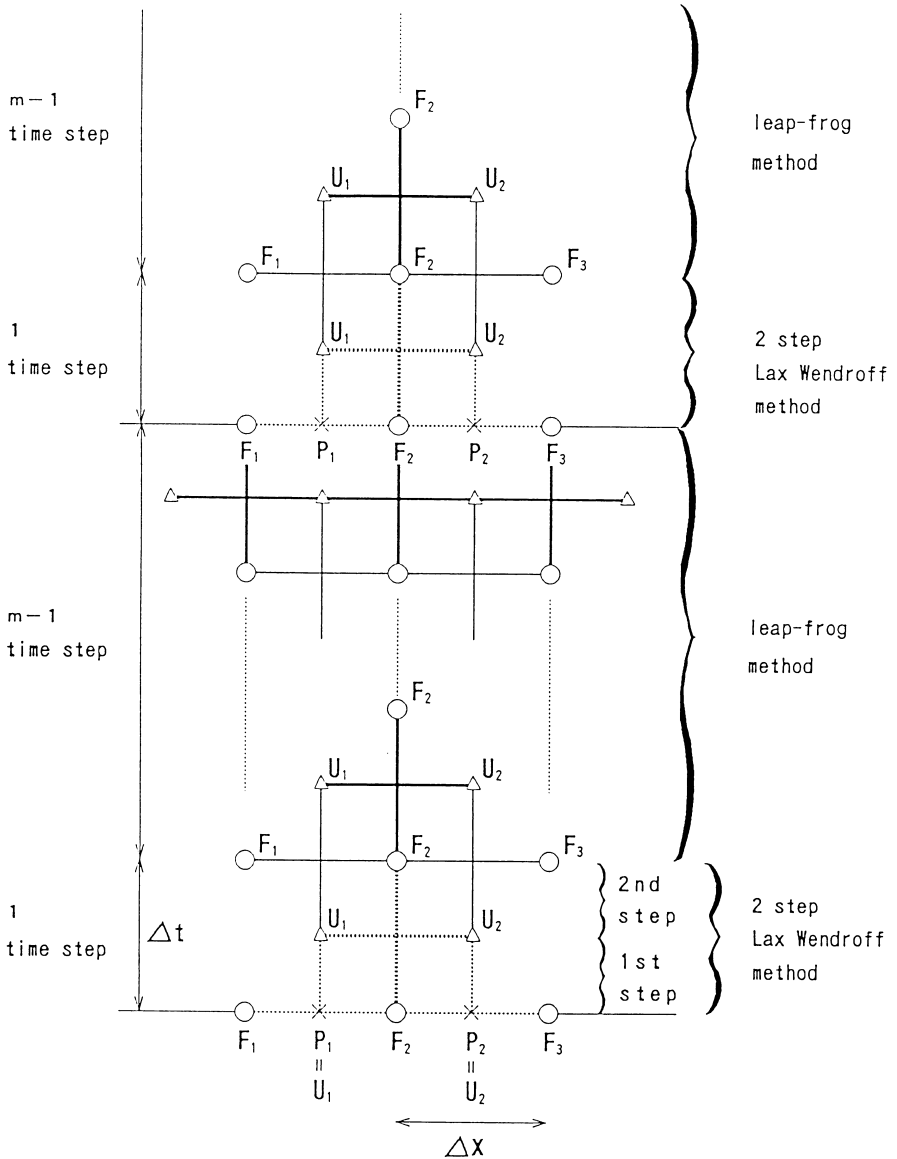
Figure 6.15: Schematic diagram of computational procedure due to a higher resolution algorithm, modified leap frog method.

Thus the amplification factor of modified leap-frog method can be given by combination of them.

$$
\begin{aligned}
A_{DLF} &= 1 - 2(1+\alpha)\delta^2 \sin^2 \frac{\kappa}{2} \\
&\quad \pm i2\delta \sin \frac{\kappa}{2}[1 - (1+\alpha)^2\delta^2 \sin^2 \frac{\kappa}{2}]^{\frac{1}{2}} \tag{6.47} \\
|A_{DLF}| &= 1 - 4\alpha\delta^2 \sin^2 \frac{\kappa}{2} \tag{6.48} \\
A_{MLF} &= A_{DLF}{}^{\frac{l-1}{l}} A_{LW}{}^{\frac{1}{l}} \tag{6.49} \\
|A_{MLF}| &= |A_{DLF}|^{\frac{l-1}{l}} |A_{LW}|^{\frac{1}{l}} \tag{6.50}
\end{aligned}
$$

where $\delta = \frac{\Delta t}{\Delta x}$, $\kappa = k\Delta x$ and A_{DLF} means the amplification factor of leap-frog method with diffusion term. The two numerical parameters in the modified leap-frog method are properly given from a test wave calculation as follows;

$$\alpha = 0.01 \sim 0.1 \quad \text{and} \quad l = 8 \sim 16.$$

An interesting feature of modified leap-frog method is that it approaches leap-frog method in a limit for larger l and does two-step Lax-Wendroff method in another limit for $l = 1$.

In Figure 6.16 are shown the 3-dimensional global simulation due to the modified leap-frog method. It is recognized that a very sharp discontinuity of bow shock or magnetopause is formed, where a large number of grid point $(N_x, N_y, N_z) = (240, 100, 100)$ and a fine spatial grid of $\Delta x = \Delta y = \Delta z = 0.25$ R_e are used. Therefore it becomes possible to simulate phenomena which are appear at the magnetopause.

6.6 Concluding Remarks

We have tried to simulate interaction between the solar wind and the earth's magnetosphere by using a 2-dimensional global MHD code in this tutorial course. And also a fundamental idea of numerical method and a extension to three dimensional version are also demonstrated. The present MHD code is a fundamental one if we neglect specular inner boundary condition and initial condition of the intrinsic dipole field. In the present MHD code we use the two-step Lax-Wendroff method and it can be considered to be a standard method because the method has been well understood for many investigators and is a typically well balanced one in the numerical diffusion and the numerical damping. In this sense, it is important to compare with the two-step Lax-Wendroff method when one develops a new numerical scheme.

When we search subjects which should be solved from the global MHD simulation in the earth's magnetosphere, we must so surprised how wide ranges
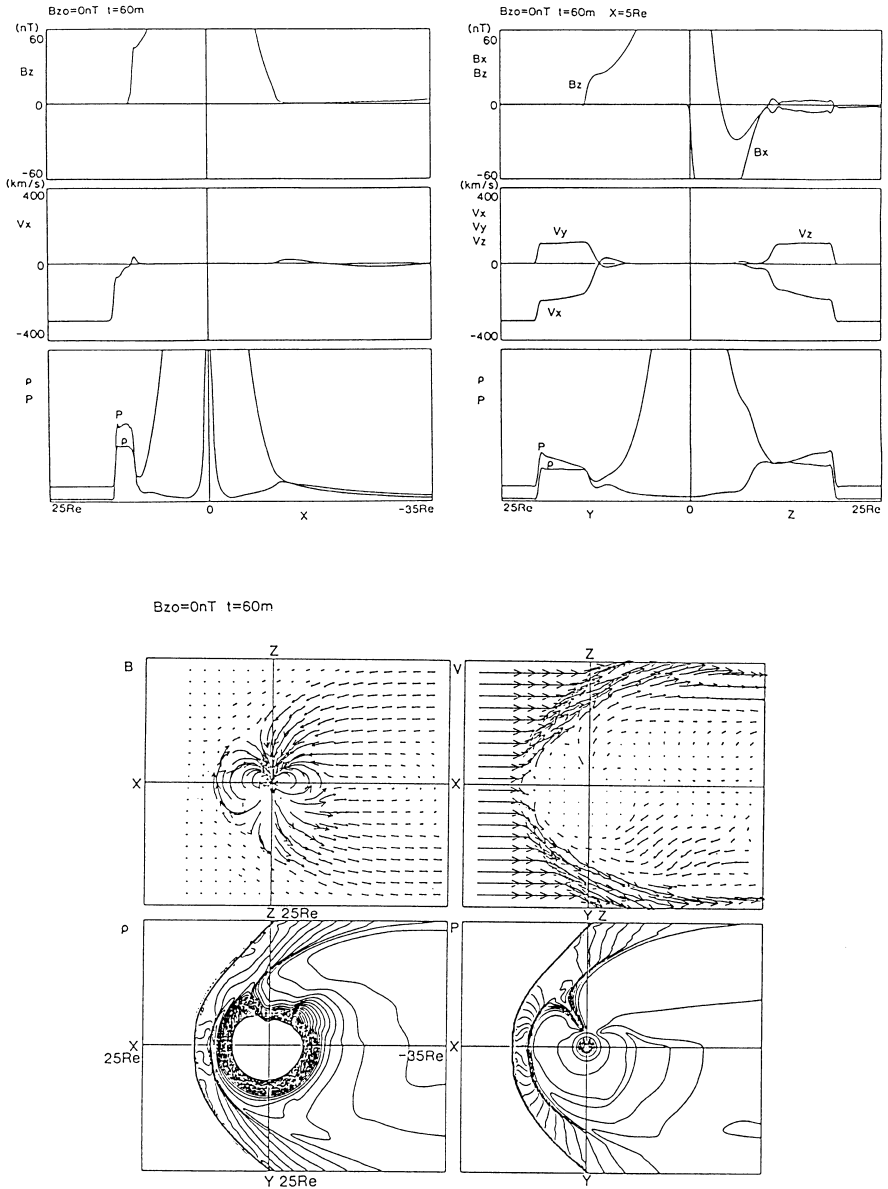
Figure 6.16: Quasi-steady state magnetospheric configuration which was simulated by the modified leap frog method for no uniform IMF. Profiles in the sun-earth line (top left panel), profiles along y-axis and z-axis at $x = 5Re$ (top right panel) and patterns in the noon-midnight and equatorial planes (bottom panel).
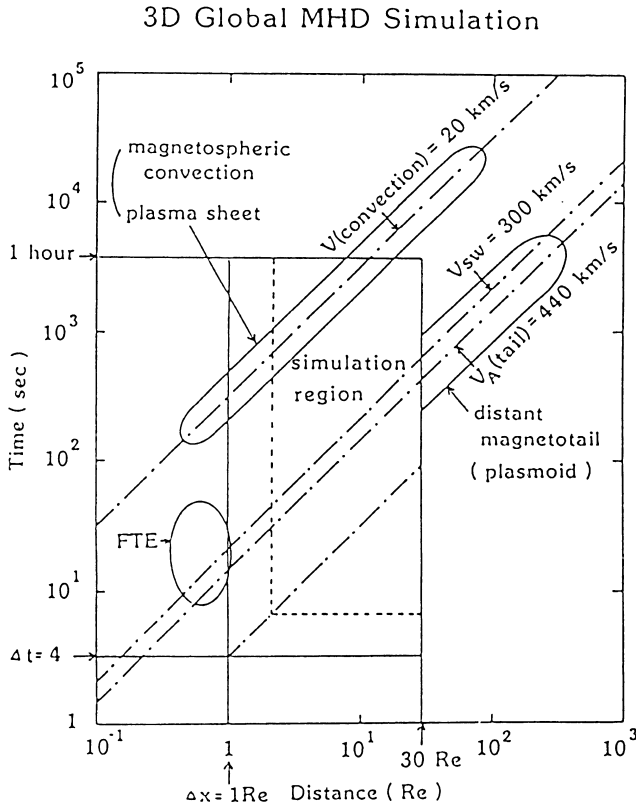
3D Global MHD Simulation

Figure 6.17: Tempral and spatial scales of the earth's magnetosperic phenomena. Time, space, and velocity scales in magnetospheric processes expand up tp 1000 times.

in time and space are necessary for research targets as is shown in Figure 6.17. The convection speed in the ionosphere is the order of 1km/s on the other hand that in the magnetosphere is 70km/s and sometimes increases up to 1000km/s in association with magnetospheric substorms. In the magnetosphere, small scale structure looks connecting with large scale structure. The processes are highly nonlinear and occurs in the inhomogeneous media. Therefore it will be also important to study phenomena of magnetospheric physics from the global MHD simulation. In particular, 3-dimensional simulation will become necessary to analyze many complicated magnetospheric processes and also space physics.

Acknowledgments

Appendix A : Note on Numerical Scheme

1. Exact solution of wave equation

Here we consider to solve a hyperbolic partial differential equation by the difference method. Let us start with the following wave equation with characteristic speed of 1,

$$\frac{\partial u}{\partial t} = \frac{\partial u}{\partial x} \tag{6.51}$$

When we use the Fourier analysis, the exact solution is calculated as

$$u = u_0 e^{i\omega t + ikx} \tag{6.52}$$

$$\omega = k. \tag{6.53}$$

Therefore we can determine an amplification factor, A for a time step advance of Δt as

$$u_i^{j+1} = A u_i^j \tag{6.54}$$

$$A = e^{i\omega \Delta t} = e^{ik\Delta t} \tag{6.55}$$

where the abbreviation of $u_i^{j+1} \equiv u(t_j + \Delta t, x_i) = u_0 e^{i\omega(t_j + \Delta t) + ikx_i}$ and $u_i^j \equiv u(t_j, x_i) = u_0 e^{i\omega t_j + ikx_i}$ is used. Moreover, by using the spatial difference, $\Delta x A$ is rewritten to

$$A = e^{ik\Delta x \frac{\Delta t}{\Delta x}} \equiv e^{i\kappa\delta} \tag{6.56}$$

where $\kappa \equiv k\Delta x$ and $\delta \equiv \Delta t/\Delta x$ are generally two important parameters to express the wave number range of $0 \leq \kappa(= k\Delta x) \leq 2\pi$ and to determine the numerical stability in the difference scheme. A difference scheme is admitted to be numerically stable if $|A| \leq 1$ is satisfied for all κ in the range of $0 \leq \kappa \equiv k\Delta x \leq 2\pi$. Of course $|A| = 1$ is valid for (A4). Here, let us define the two parameters of the absolute value, $|A|$ and the normalized phase, θ (or the phase velocity, v_{ph}) to study the amplification factor in the difference scheme in detail.

$$absolute \quad value \qquad |A| \tag{6.57}$$

$$phase \quad \theta = \frac{1}{\delta} \tan^{-1}(Im\ A/Re\ A) \tag{6.58}$$

$$phase \quad velocity \quad v_{ph} = \theta/\kappa \tag{6.59}$$

where $Im\ A$ and $Re\ A$ mean the imaginary part and real part of A. For the exact solution in (6.56) the following values,

$$|A| = 1 \tag{6.60}$$

$$\theta = \frac{1}{\delta}\tan^{-1}(\tan\kappa\delta) = \kappa \tag{6.61}$$

$$v_{ph} = \theta/\kappa = 1 \tag{6.62}$$

are obtained.

Remarks for the exact analytical solution of wave equation:

1. $|A|$ is always 1.

2. θ is proportional to $\kappa(=k\Delta x)$, or $v_{ph} =1$.

2. Basic consideration of explicit and implicit difference schemes

Let us introduce the following difference scheme in order to solve (6.51)

$$\frac{u_i^{j+1} - u_i^j}{\Delta t} = \alpha\frac{u_{i+1}^{j+1} - u_{i-1}^{j+1}}{2\Delta x} + (1-\alpha)\frac{u_{i+1}^j - u_{i-1}^j}{2\Delta x} \tag{6.63}$$

where $0 \le \alpha \le 1$.

$$lu_i^{j+1} - \alpha\frac{\Delta t}{2\Delta x}(u_{i+1}^{j+1} - u_{i-1}^{j+1}) = u_i^j + (1-\alpha)\frac{\Delta t}{2\Delta x}(u_{i+1}^j - u_{i-1}^j) \tag{6.64}$$

$$\{1 - \alpha\frac{\Delta t}{2\Delta x}(e^{i\kappa} - e^{-i\kappa})\}u_i^{j+1} = \{1 + (1-\alpha)\frac{\Delta t}{2\Delta x}(e^{i\kappa} - e^{-i\kappa})\}u_i^j \tag{6.65}$$

From (6.54), we can calculate

$$A = \frac{1 + (1-\alpha)i\delta\sin\kappa}{1 + \alpha i\delta\sin\kappa} \tag{6.66}$$

$$|A|^2 = \frac{1 + (1-\alpha)^2\delta^2\sin^2\kappa}{1 + \alpha^2\delta^2\sin^2\kappa} \tag{6.67}$$

Therefore $\alpha \ge \frac{1}{2}$ is given from $|A|^2 \le 1$.

$\begin{array}{lll} |A| < 1 & \text{for}\ \ \frac{1}{2} < \alpha \le 1 & \Rightarrow\ \ \text{numerically stable} \\ |A| = 1 & \text{for}\ \ \alpha = \frac{1}{2} & \Rightarrow\ \ \text{marginally stable} \\ |A| > 1 & \text{for}\ \ 0 \le \alpha < \frac{1}{2} & \Rightarrow\ \ \text{numerically unstable} \end{array}$ The explicit scheme

is only for $\alpha = 0$ and the implicit scheme is for $0 < \alpha \le 1$.

Remarks for explicit and implicit schemes

1. simple explicit scheme is unstable ($\alpha = 0$).

2. time central scheme is marginally stable ($\alpha = \frac{1}{2}$).

3. some implicit scheme is unconditionally stable ($\frac{1}{2} < \alpha \le 1$).

3. Leap–frog scheme (complete time central scheme)
Ordinary leap–frog scheme

$$\frac{u_i^{j+1} - u_i^{j-1}}{2\Delta t} = \frac{u_{i+1}^j - u_{i-1}^j}{2\Delta x} \tag{6.68}$$
$$(A - A^{-1})u_i^j = \delta(e^{i\kappa} - e^{-i\kappa})u_i^j$$

$$\therefore \ A^2 - 2\delta i \sin\kappa - 1 = 0 \tag{6.69}$$

$$A = \pm\sqrt{1 - \delta^2 \sin^2\kappa} + i\delta\sin\kappa |A|^2 = 1. \tag{6.70}$$

Modified leap–frog scheme with a half spatial grid size

$$\frac{u_i^{j+1} - u_i^j}{\Delta t} = \frac{u_{i+\frac{1}{2}}^{j+\frac{1}{2}} - u_{i-\frac{1}{2}}^{j+\frac{1}{2}}}{\Delta x} \tag{6.71}$$

$$\therefore \ A - 2i\delta \sin\frac{\kappa}{2}A^{\frac{1}{2}} - 1 = 0 \tag{6.72}$$

$$A^{\frac{1}{2}} \ = \ \pm\sqrt{1 - \delta^2 \sin^2\frac{\kappa}{2}} + i\delta\sin\frac{\kappa}{2} \tag{6.73}$$
$$|A| \ = \ 1. \tag{6.74}$$

Remarks for leap–frog scheme

1. $|A|$ is always 1.

2. modified scheme has higher numerical accuracy.

4. Two step Lax–Wendroff scheme
Ordinary two-step Lax–Wendroff scheme
1st step

$$u_i^{j+\frac{1}{2}} = \frac{u_{i+1}^j + u_{i-1}^j}{2} + \frac{\Delta t}{4\Delta x}(u_{i+1}^j - u_{i-1}^j) \tag{6.75}$$

2nd step

$$u_i^{j+1} \ = \ u_i^j + \frac{\Delta}{2\Delta x}(u_{i+1}^{j+\frac{1}{2}} - u_{i-1}^{j+\frac{1}{2}}) \tag{6.76}$$
$$u_i^{j+1} \ = \ A \, u_i^j$$
$$A \ = \ 1 + i(\frac{\delta}{2})\sin 2\kappa + (\frac{\delta}{2})^2(\cos 2\kappa - 1) \tag{6.77}$$
$$|A|^2 \ = \ 1 + \{(\frac{\delta}{2})^4 - (\frac{\delta}{2})^2\}(\cos 2\kappa - 1)^2 \tag{6.78}$$

Therefore $|A| \le 1$ is satisfied for $0 \le \frac{\delta}{2} (= \frac{\Delta t}{2\Delta x}) \le 1$ and for all κ.

Modified two-step Lax-Wendroff scheme
1st step

$$u_{i+\frac{1}{2}}^{j+\frac{1}{2}} = \frac{u_{i+1}^j + u_i^j}{2} + \frac{\Delta t}{2\Delta x}(u_{i+1}^j - u_i^j) \tag{6.79}$$

2nd step

$$u_i^{j+1} = u_i^j + \frac{\Delta t}{\Delta x}(u_{i+\frac{1}{2}}^{j+\frac{1}{2}} - u_{i-\frac{1}{2}}^{j+\frac{1}{2}}) \tag{6.80}$$

$$A = 1 + i\delta \sin\kappa + \delta^2(\cos\kappa - 1) \tag{6.81}$$

$$|A|^2 = 1 + (\delta^4 - \delta^2)(\cos\kappa - 1)^2 \tag{6.82}$$

Therefore $|A| \le 1$ is satisfied for $0 \le \delta (= \frac{\Delta t}{\Delta x}) \le 1$ and for all κ.

Remarks for the two-step Lax–Wendroff scheme

1. $|A| \le 1$ is satisfied for $0 \le \delta \le 2$ (or 1 for modified scheme).

2. modified scheme has higher numerical accuracy.

Appendix B : Comments on Runge–Kutta–Gill Method

We have studied several higher order numerical schemes such as modified leap frog method, iterative Lax–Wendroff method, Runge–Kutta method, Runge–Kutta–Gill method in order to improve the numerical accuracy in the global MHD model. In those schemes, we will discuss the Runge–Kutta–Gill (RKG) method which is applied to a partial differential wave equation in comparison with the 2 step Lax–Wendroff (2LW) method. In conclusion we should say that the RKG method with the second order spatial difference has not higher numerical accuracy than the 2LW method in the order. The RKG method with the fourth order spatial difference has a higher numerical accuracy of the fourth order. Let us start with the following simple differential wave equation,

$$\frac{\partial u}{\partial t} = \frac{\partial u}{\partial x} \tag{6.83}$$

The amplification factor of the exact solution in Fourier analysis $(e^{iwt+ikx})$ is given by

$$\begin{aligned} A_E &= e^{iw\Delta t} = e^{i\frac{\Delta t}{\Delta x}k\Delta x} = e^{i\delta\theta} \\ &= \cos\delta\theta + i\sin\delta\theta \\ &= \{1 - \frac{1}{2}(\delta\theta)^2 + \frac{1}{24}(\delta\theta)^4 - \cdots \quad \} \\ &\quad + i\{\delta\theta - \frac{1}{6}(\delta\theta)^3 + \frac{1}{120}(\delta\theta)^5 - \cdots \quad \} \end{aligned} \tag{6.84}$$

Solution of the Wave Equation due to
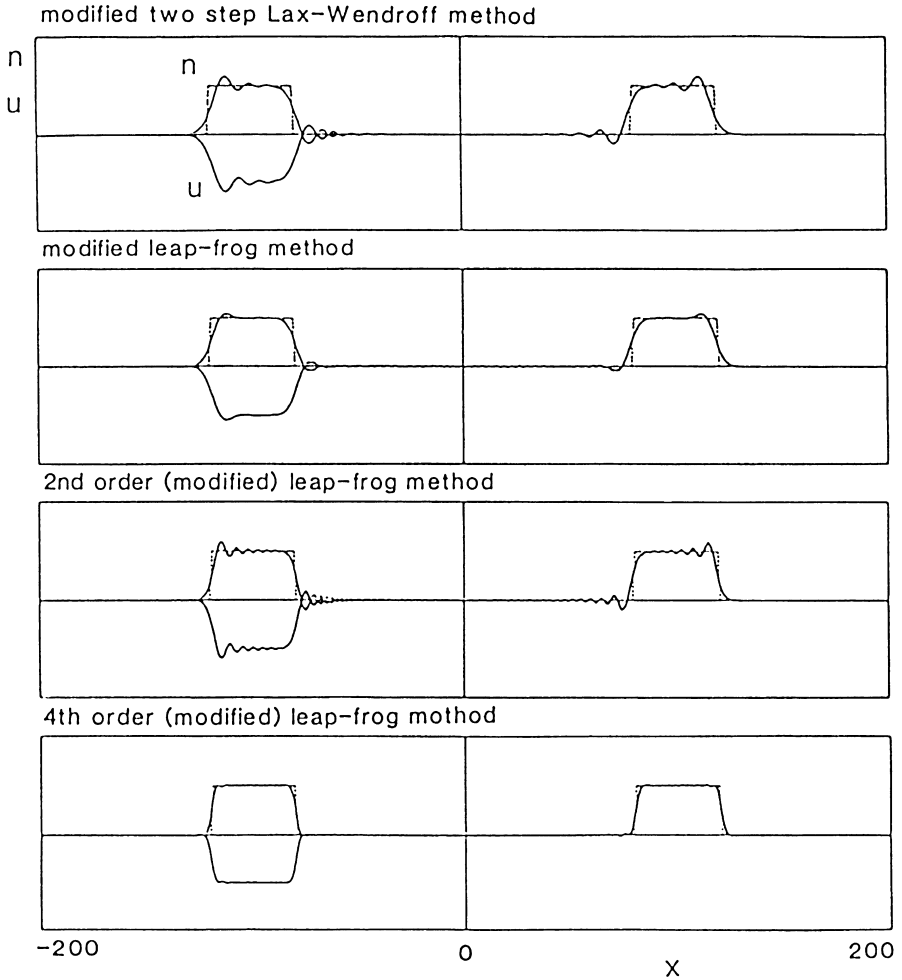
Modified Leap-Frog Method

Figure 6.18: Numerical simulation of the wave equation by using the modified two-step Lax-Wendroff method and leap-frog method.
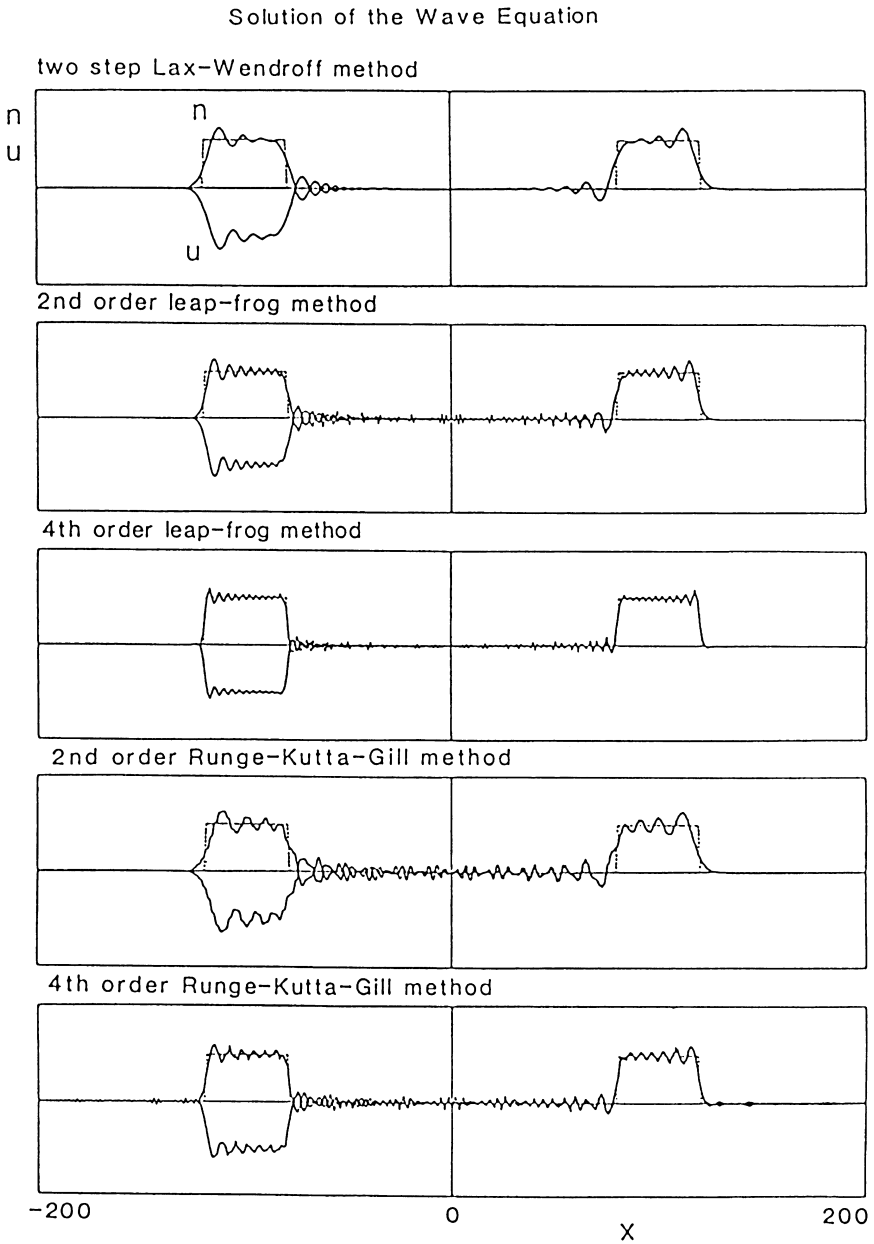
Figure 6.19: Numerical simulation of the wave equation by using several numerical schemes.
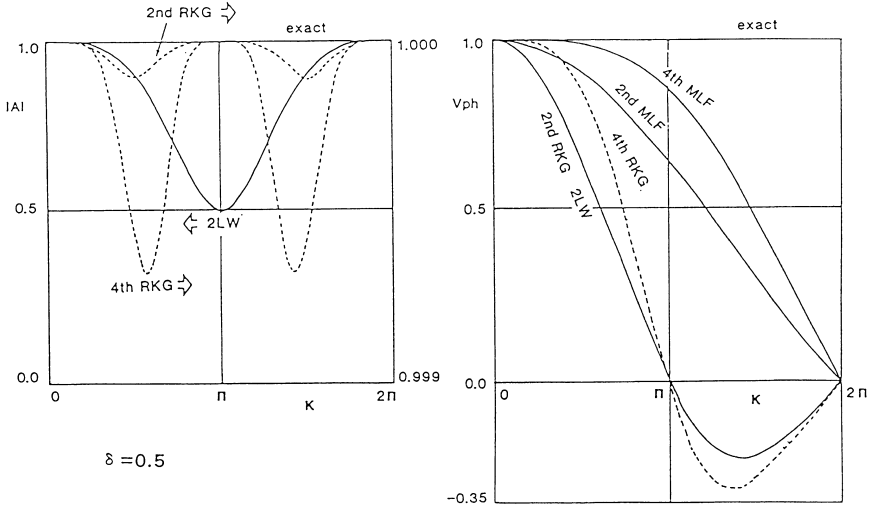
Figure 6.20: Absolute value and phase velocity of the amplification factor on 2 step Lax-Wendroff (2LW) and Runge-Kutta-Gill (RKG) methods.

where, $\delta = \frac{\Delta t}{\Delta x}$, $\theta = k\Delta x$, and Δt and Δx stand for the temporal and spatial grid intervals in the difference scheme. Therefore, $|A_E| = 1$ and the phase of A_E is given by $\delta\theta$. The absolute value of the amplification factor keeps unity and the phase is proportional to $\theta = k\Delta x$. The amplification factor of the 2LW method is

$$A_{2LW} = 1 + \delta^2(\cos\theta - 1) + i\delta\sin\theta \qquad (6.85)$$

$$|A_{2LW}|^2 = 1 + (\delta^4 - \delta^2)(\cos\theta - 1)^2 \qquad (6.86)$$

and that of the RKG method with the second order spatial difference, $\frac{\partial u}{\partial t} = \frac{\partial u_i}{\partial x} = \frac{u_{i+1}^j - u_{i-1}^j}{2\Delta x}$ is

$$A_{RKG} = 1 - \frac{1}{2}\delta^2\sin^2\theta + \frac{\delta^4}{24}\sin^4\theta + i(\delta\sin\theta - \frac{1}{6}\delta^3\sin^3\theta) \quad (6.87)$$

$$|A_{RKG}|^2 = 1 - \frac{\delta^6}{72}\sin^6\theta + \frac{\delta^8}{576}\sin^8\theta \qquad (6.88)$$

Therefore, the RKG method seems to have a much higher numerical accuracy when we look at $|A_{RKG}|$ only. However, the complex amplification factors in (6.85) and (6.87) can be expanded as follows;

$$A_{2LW} \qquad = 1 - \tfrac{1}{2}\delta^2\theta^2 + \tfrac{\delta^2\theta^4}{24} + \cdots\cdots$$
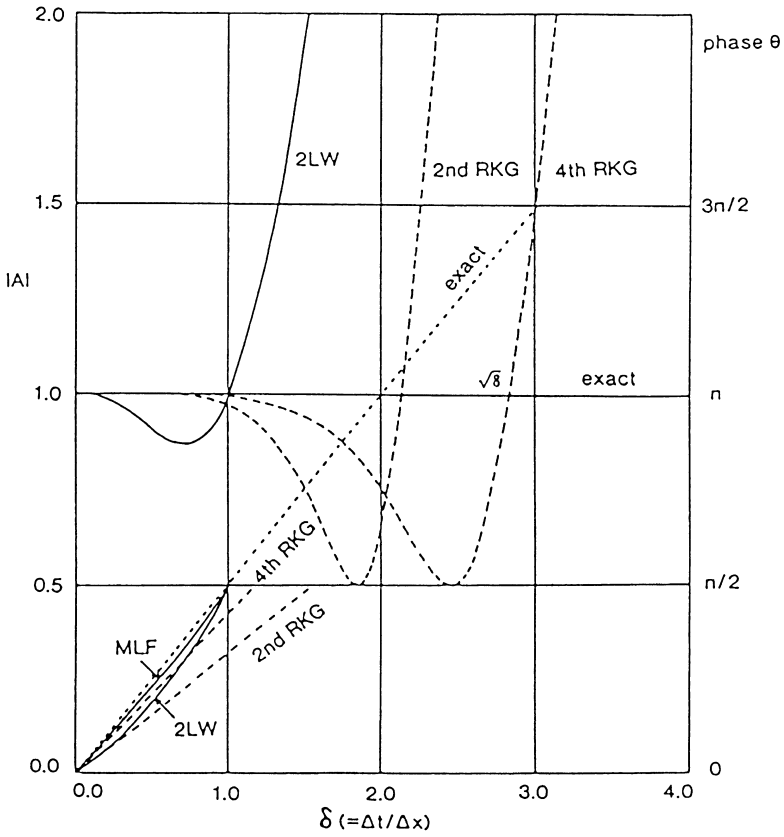$$+ i\{\delta\theta - \tfrac{\delta\theta^3}{6} + \cdots\cdots \qquad\qquad \} \qquad (6.89)$$

Figure 6.21: Absolute value of the amplification factor versus $\delta(= \Delta t/\Delta x)$ on 2LW and RKG methods.

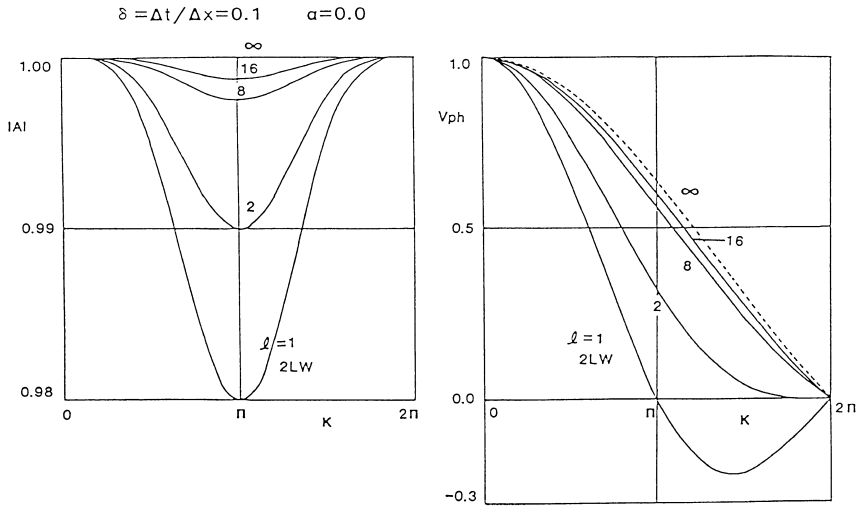$\delta = \Delta t / \Delta x = 0.1$ $a = 0.0$

Figure 6.22: Absolute value and phase velocity of the amplification factor on the modified leap-frog method with no explicit damping rate $\alpha = 0$.
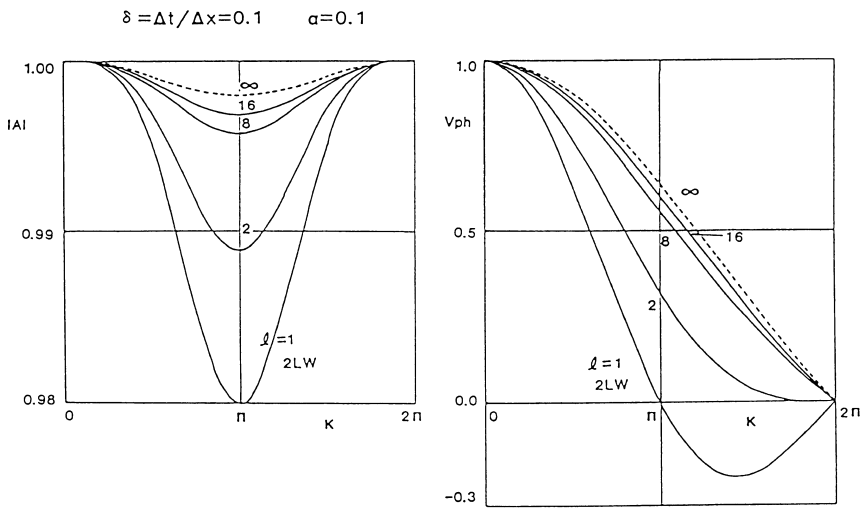
$\delta = \Delta t / \Delta x = 0.1$ $a = 0.1$

Figure 6.23: Absolute value and phase velocity of the amplification factor on the modified leap-frog method with no a finite damping rate $\alpha = 0.1$.

$$
\begin{aligned}
A_{RKG} \quad &= 1 - \tfrac{1}{2}\delta^2(\theta^2 - \tfrac{1}{3}\theta^4) + \tfrac{\delta^4\theta^4}{24} + \cdots\cdots \\
&+ i\{\delta(\theta - \tfrac{\theta^3}{6}) + \cdots\cdots - \tfrac{1}{6}\delta^3\theta^3 + \cdots\cdots \qquad\qquad \}
\end{aligned}
\tag{6.90}
$$

Therefore, we can see that numerical errors in the same order appear in both A_{2LW} and A_{RKG} in comparison with the exact amplification factor, A_E in (B2). That is, $|A_{RKG}|$ is less than unity for $\delta < \sqrt{8}$ and very close to unity. However, the phase of A_{RKG} is the same order as that of A_{2LW}, and the numerical error of the phase in the RKG method rather increases than that in the 2LW method. It might be possible that the RKG method is an improved method because the wave damping becomes very small keeping the same order numerical accuracy in phase as the 2LW method. Moreover, we can say that one can use a large $\delta = \frac{\Delta t}{\Delta x}(< \sqrt{8})$ and the spatial difference in the RKG method is direct and simple. However, I do not agree that the second order RKG method has a higher accuracy than the 2LW method. It is not generally correct that simulation results by the RKG method are valid because of smaller damping of MHD waves even for larger $\theta = k\Delta x$. This is because the waves with smaller damping for larger θ propagate with incorrect phase velocity. Therefore, it might be possible to say that simulation results for some problems by the RKG method are less valid for smaller scale than those by the 2LW method because the waves for larger θ have incorrect phase velocity and do not damp. In the RKG method, we can choose the fourth order difference in space as follows;

$$
\frac{\partial u}{\partial t} = \frac{\partial u}{\partial x} = \frac{8(u_{i+1} - u_{i-1}) - (u_{i+2} - u_{i-2})}{12\Delta x}
\tag{6.91}
$$

then we can eliminate the numerical errors shown in (6.90) and the numerical accuracy become higher up to the order of $\delta^4\theta^4$. We need a further effort to apply the fourth order Runge–Kutta–Gill method to the global 3–dimensional MHD model.

References

Akasofu, S.-I., What is a magnetospheric substorm, in *Dynamics of the Magnetosphere*, S.-I. Akasofu, ed., D. Reidel, Bigham, Mass, 1980.

Birn, J., Three-dimensional computer modeling of dynamic reconnection in the magnetotail: Plasmoid signatures in the near and distant tail, in *Magnetic Reconnection in Space and Laboratory Plasmas, Geophys. Monogr.*, *30*, E. W. Hones, ed., 264, 1984.

Brecht, S. H., J. G. Lyon, J. A. Fedder, and K. Hain, A simulation study of east-west IMF effects on the magnetosphere, *Geophys. Res. Lett.*, *8*, 397, 1981.

Brecht, S. H., J. G. Lyon, J. A. Fedder, and K. Hain, A time dependent three dimensional simulation of the earth's magnetosphere: Reconnection events, *J. Geophys. Res.*, *87*, 6098, 1982.

Dungey, J. W., Interplanetary magnetic field and the auroral zones, *Phys. Rev. Lett.*, *6*, 47, 1961.

Erickson, G. M., On the cause of x-line formation in the near-Earth plasma sheet: results of adiabatic convection of plasma sheet plasma, in *Magnetic Reconnection in Space and Laboratory Plasmas, Geophys. Monogr.,30*, E. W. Hones, ed., 296, 1984.

Erickson, G. M., and R. A. Wolf, Is steady convection possible in the Earth's magnetotail?, *Geophys. Res. Lett.,7*, 897, 1980.

Fedder, J. A., and J. G. Lyon, The solar wind-magnetosphere- ionosphere current voltage relationship, *Geophys. Res. Lett.,14*, 880, 1987.

Fedder, J. A., S. H. Brecht and J. G. Lyon, MHD simulation of a comet, *NRL Memo. Rpt., 5397*, 1984.

Frank, L. A., J. D. Craven, J. L. Burch, and J. D. Winningham, Polar views of the Earth's aurora with Dynamics Explorer, *Geophys. Res. Lett.*, *9*, 1001, 1982.

Frank, L. A., J. D. Craven, D. A. Gurnett, S. D. Shawhan, D. R. Weimer, J. L. Burch, J. D. Winningham, C. R. Chappell, J. H. Waite, R. A. Hellis, N. C. Maynard, M. Sugiura, W. K. Peterson, and E. G. Shelly, The theta aurora, *J. Geophys. Res.*, *91*, 3177, 1986.

Hones, E. W., Jr., Plasma sheet behavior during substorms, in *Magnetic Reconnection in Space and Laboratory Plasmas, Geophys. Monogr., 30*, E. W. Hones, ed., 178, 1984.

Hughes, W. J., and D. G. Sibeck, On the 3-dimensional structure of plasmoids, *Geophys. Res. Lett.*, *14*, 636, 1987.

Iijima, T., and T. A. Potemra, The amplitude distribution of field-aligned current at northern high latitudes observed by TRIAD, *J. Geophys. Res.*, *81*, 2165, 1976.

La Belle-Harmer, A. L., Z. F. Fu, and L. C. Lee, A mechanism for patchy reconnection at the dayside magnetopause, *Geophys. Res. Lett.*, *15*, 152, 1988.

Leboeuf, J. N., T. Tajima, C. F. Kennel, and J. M. Dawson, Global simulations of the time-dependent magnetosphere, *Geophys. Res. Lett.*, *5*, 609, 1978.

Leboeuf, J. N., T. Tajima, C. F. Kennel, and J. M. Dawson, Global simulations of the three dimensional magnetosphere, *Geophys. Res. Lett.*, *8*, 257, 1981.

Lee, L. C., and Z. F. Fu, A theory of magnetic flux transfer at the Earth's dayside magnetopause, *Geophys. Res. Lett.*, *12*, 105, 1985.

Linker, J. A., M. G. Kivelson, and R. J. Walker, An MHD simulation of plasma flow past Io: Alfvén and slow mode perturbations, *Geophys. Res. Lett.*, in press, 1988.

Lyon, J. G., S. H. Brecht, J. A. Fedder, and P. J. Palmadesso, The effect on the earth's magnetotail from shocks in the solar wind, *Geophys. Res. Lett.*, *7*, 712, 1980.

Lyon J. G., S. H. Brecht, J. D. Huba, J. A. Fedder, and P. J. Palmadesso, Computer simulation of geomagnetic substorm, *Phys. Rev. Lett.*, *46*, 1038,

1981.

Lyon, J. G., J. A. Fedder, and J. D. Huba, The effects of different resistivity models on magnetotail dynamics, *J. Geophys. Res.*, *91*, 8057, 1986.

McPherron, Magnetospheric substorms, *Rev. Geophys and Space Phys.*, *17*, 657, 1979.

Ogino, T., A three dimensional MHD simulation of the interaction of the solar wind with the earth's magnetosphere: The generation of field aligned currents, *J. Geophys. Res.*, *91*, 6791, 1986.

Ogino, T., and R. J. Walker, A magnetohydrodynamic simulation of the bifurcation of the tail lobes during intervals with a northward interplanetary magnetic field, *Geophys. Res. Lett.*, *11*, 1018, 1984.

Ogino, T., and R. J. Walker, Magnetic flux ropes in 3-dimensional MHD simulations, in *Physics of Magnetic Flux Ropes, Geophys, Monogr. Ser.*, *58*, C. T. Russell, E. R. Priest, and L. C. Lee, ed., AGU, Washington D. C., 669, 1990.

Ogino, T., R. J. Walker, and M. Ashour-Abdalla, An MHD simulation of the interaction of the solar wind with the outflowing plasmas from a comet, *Geophys. Res. Lett.*, *13*, 929, 1986*a*.

Ogino, T., R. J. Walker, and M. Ashour-Abdalla, A three dimensional MHD simulation of the interaction of the solar wind with Comet Halley, UCLA IGPP Publ, 3047, *J. Geophys. Res.*, *93*, 9568, 1988*a*.

Ogino, T., R. J. Walker, M. Ashour-Abdalla, and J. M. Dawson, An MHD simulation of B_y dependent magnetospheric convection and field-aligned currents during northward IMF, *J. Geophys. Res.*, *90*, 10835, 1985.

Ogino, T., R. J. Walker, and M. Ashour-Abdalla, A magnetohydrodynamic simulation of the formation of magnetic flux tubes at the earth's dayside magnetopause, *Geophys. Res. Lett.*, *16*, 155, 1989*a*.

Ogino, T., R. J. Walker, M. Ashour-Abdalla, and J. M. Dawson, An MHD simulation of the effects of the interplanetary magnetic field B_y component on the interaction of the solar wind with the earth's magnetosphere during southward interplanetary magnetic field, *J. Geophys. Res.*, *91*, 10029, 1986*b*.

Ogino, T., R. J. Walker, and M. Ashour-Abdalla, The effects of dipole tilt on magnetotail structure and dynamics, *Proceedings of the Research Institute of Atmospherics Nagoya University*, *36*, 29, 1989*b*.

Ogino, T., R. J. Walker, and M. Ashour-Abdalla, A computer model of the Earth's magnetosphere, *Proceedings of the Research Institute of Atmospherics Nagoya University*, *35*, 1, 1988*b*.

Potter, D., *Computational Physics*, p.304, John Wiley, Rochester, New York, 1970.

Rostoker, G., and T. Eastman, A boundary layer model for magnetospheric substorms, *J. Geophys. Res.*, *92*, 12, 187, 1987.

Sato, T., T. Shimada, M. Tanaka, T. Hayashi, and K. Watanabe, Formation of field-twisting flux tubes on the magnetopause and solar wind particle entry into the magnetosphere, *Geophys. Res. Lett.*, *13*, 801, 1986.

Sato, T., Auroral physics, in *Magnetospheric Plasma Physics*, A. Nishida, ed., 197, D. Reidel Publ. Co., Hingham, Ma., 1982.

Schmidt, H. U., and R. Wegmann, MHD-calculations for cometary plasmas, *Comp. Phys. Comm.*, *19*, 309, 1980.

Schmidt, H. U., and R. Wegmann, Plasma flow and magnetic fields in Comets, *Comets*, L. L. Wilkering, ed. University of Arizona Press, Tucson, 1982.

Scholer, M., Magnetic flux transfer at the magnetopause, *Geophys. Res. Lett.*, *15*, 291, 1988.

Shi, Y., C. C. Wu, and L. C. Lee, A study of multiple X line reconnection at the dayside magnetopause, *Geophys. Res. Lett.*, *15*, 295, 1988.

Southwood, D. J., C. J. Farrugia, and M. A. Saunders, What are flux transfer events?, *Planet. Space Sci.,* *92*, 8613, 1987.

Spence, H. E., M. G. Kivelson, and R. J. Walker, Magnetotail plasma Pressures: Empirical Models, submitted to *J. Geophys. Res.*, 1988.

Sydora, R. D., and J. Raeder, A particle MHD simulation approach with application to a global comet-solar wind interaction model, *Cometary and Solar Plasma Physics*, B. Buti, ed., World Scientific Publishing Co., 1987.

Tsyganenko, N. A., Global quantitative models of the geomagnetic field in the cislunar magnetosphere for different disturbance levels, *Planet. Space Sci.*, *35*, 1347, 1987.

Vasyliunas, V. M., Fundamentals of current description, in *Magnetospheric Currents Geophys. Monogr. Ser.*, *28*, T. A. Potemra, ed., 63, AGU, Washington, D. C., 1984.

Walker, R. J., and T. Ogino, A magnetohydrodynamic simulation of the interaction of the solar wind with the Jovian magnetosphere (abstract), *2nd Neil Brice Memorial Symposium*, 3, 1986.

Walker R. J., and T. Ogino, Field-aligned currents and magnetospheric convection: A comparison between MHD simulations and observations, in *Modeling Magnetospheric Plasma, Geophys, Monogr. Ser.*, *44*, T. E. Moore and J. H. Waite, Jr., ed., AGU, Washington D. C., 39, 1988.

Walker, R. J., T. Ogino, and M. Ashour-Abdalla, A magnetohydrodynamic simulation of reconnection in the magnetotail during intervals with southward interplanetary magnetic field, in *Magnetotail Physics*, A. T. Y. Lui, ed., Johns Hopkins University Press, Baltimore, 183, 1987.

Walker, R. J., T. Ogino, and M. Ashour-Abdalla, A global magnetohydrodynamic model of magnetospheric substorms, *SPI Conference Proceedings and Reprint Series*, in press, 1988*a*.

Walker, R. J., T. Ogino, and M. Ashour-Abdalla, Simulating the magnetosphere: The structure of the magnetotail, in *Geophys. Monogr. Ser.*, J. Burch and J. H. Waite, eds., AGU, Washington D. C., in press, 1988*b*.

Watanabe, K., and T. Sato, Global simulation of the solar wind – magnetosphere interaction: The importance of its numerical validity, *J. Geophys. Res.*, *95*, 75, 1990.

Wegmann, R., H. U. Schmidt, W. F. Huebner, and D. C. Boice, Cometary MHD and Chemistry, *Astron., Astrophys.*, *187*, 339, 1987.

Wu, C. C., Shape of the magnetosphere, *Geophys. Res. Lett.*, *10*, 545, 1983.

Wu, C. C., The effects of dipole tilt on the structure of the magnetosphere, *J. Geophys. Res.*, *89*, 12, 1984.

Wu, C. C., R. J. Walker, and J. M. Dawson, A three dimensional MHD model of the earth's magnetosphere, *Geophys. Res. Lett.*, *8*, 523, 1981.